Comparative framework for spatially explicit urban growth modeling for monitoring urban land-use efficiency and sustainable urban development (SDG 11.3.1): a study on Kolkata metropolitan area, India

Sk Mithun, Mehebub Sahana, Subrata Chattopadhyay, Soumendu Chatterjee, Jaidul Islam & Romulus Costache

Taylor & Francis
Taylor & Francis Group

Check for updates

Comparative framework for spatially explicit urban growth modeling for monitoring urban land-use efficiency and sustainable urban development (SDG 11.3.1): a study on Kolkata metropolitan area, India

Sk Mithun[a] (ID), Mehebub Sahana[b], Subrata Chattopadhyay[c], Soumendu Chatterjee[d], Jaidul Islam[e] and Romulus Costache[f] (ID)

[a]Department of Geography, Haldia Government College, Haldia, West Bengal, India; [b]Department of Geography, University of Manchester, Manchester, UK; [c]Department of Architecture and Regional Planning, Indian Institute of Technology Kharagpur, Kharagpur, India; [d]Department of Geography, Presidency University, Kolkata, West Bengal, India; [e]Department of Geography, PRMS Mahavidyalaya, Bankura, West Bengal, India; [f]Department of Civil Engineering, Transilvania University of Brasov, Brasov, Romania

ABSTRACT

The present study attempts to model the spatiotemporal urban growth of the Kolkata metropolitan area (KMA), India, in a comparative modeling framework using three (remote sensing and geographic information system) RS-GIS integrated techniques, namely stochastic-choice Markov-chain (STCHOICE), cellular automata-Markov (CA-MARKOV), and multi-layer perceptron neural network (MLPNN) coupled with Markov-chain approaches intending to monitor land-use efficiency defined by United Nations for sustainable urban development in KMA. In order to find out the best modeling approach, each of the three techniques is engaged in modeling KMA's growth, and the model thus obtained is employed to predict future growth. The MLPNN (Kappa = 0.9025) appears to be a considerably better approach as compared to the other two approaches: CA-MARKOV (Kappa = 0.6941) and STCHOICE (Kappa = 0.5392). The MLPNN simulated urban growth for 2036 reveals that the urban built-up cover is expected to be about 55% from that of 31% in 2016 due to the significant conversion of other land covers. The study reveals that urban and peri-urban areas do not have a similar pattern of land consumption and land-use efficiency in KMA. The central KMA reflects better land-use efficiency due to the compact built-up growth compared to the periphery reflecting leapfrog growth as a result of rapid urban sprawling.

HIGHLIGHTS

- Predicted future urban growth in Kolkata Metropolitan Area (KMA) using comparative modeling framework
- Monitored urban land use efficiency (SDG 11.3.1) for sustainable urban development in KMA
- The study reveals that urban and peri-urban land consumption and land use efficiency are different

CONTACT Mehebub Sahana ✉ mehebubsahana@gmail.com

- Identified most influential driving factors from the selected factors responsible for the spatial pattern of urban expansion in KMA

1. Introduction

Presently, more than half of the global population lives in urban areas, and 6 out of 10 people would be city dwellers by 2030. World cities occupy only 3% of the planet's surface yet consume 75% of the world's energy and emit 80% of global carbon dioxide emission (Estoque et al. 2021; Estoque and Murayama 2014). In the near future, about 95% of urban expansion is expected to take place in developing countries (UN, 2015). Supply of fresh water, sewage systems, air quality, and public health are all under stress as a result of rapid urbanization. Unplanned urban sprawl can hurt national development and global sustainability. The United Nations (UN) Agenda for Sustainable Development set a total of 17 sustainable development goals (SDG), 169 targets, and 232 quantifiable indicators to be achieved by 2030 (UN, 2015, 2017). UN SDG 11.3 focuses on sustainable cities and aims at "making cities inclusive, safe, resilient and sustainable." The SDG indicator 11.3.1, "Ratio of land consumption rate to the population growth rate (LCRPGR)," used to identify land-use efficiency (LUE) defined as amount of land used for urban land uses, which typically entails the conversion of non-urban to urban impervious surfaces (Li et al. 2021). To be more explicit, SDG indicator 11.3.1 measures the ratio between the rate at which cities and urban areas grow and the rate at which their people expand in order to assess how effectively cities and urban regions utilize land (UN-Habitat 2016, 2018a; Estoque et al. 2021; Rienow et al. 2022).

Thus, SDG indicator 11.3.1 signifies the relationship population and urban form. The size, area, and configuration of a city are considered to be its physical characteristics. A city's growth rate is compared to population growth to determine if it is growing faster, slower, or at the same rate (Laituri et al. 2021). Excessive urban growth measured in terms of urban built-up spread in relation to population increase leads to decline LUE (UN-Habitat, 2016). As a result, in order to increase LUE, the LCRPGR should be smaller than one with a declining trend over time (UN-Habitat 2018a; Melchiorri et al. 2019; Wang et al. 2020). The imbalance population growth to city's physical growth may create the access to transportation networks, services, and environmental sustainability challenging. Measuring LCRPGR allows urban planners and decision-makers to estimate the demand for ecosystem products and services, discover new areas for urban growth, and support long-term sustainable development effectively (UN-Habitat 2018b; Estoque et al. 2021). SDGI 11.3.1 supports the assessment and tracking of population increase and city expansion in areas where local data is required for planning and development activities, the provision of basic services, and the implementation of sustainable policies (Laituri et al. 2021). LUE trends can also be discerned by analyzing LCRPGR data over a period of time (Schiavina et al. 2019; Wang et al. 2020). As a result, tracking the indicator is critical not just for understanding spatiotemporal patterns of urban growth and formulating policies but also for encouraging sustainable urbanization (UN-Habitat 2018a; Rienow et al. 2022).

Modeling spatiotemporal urban growth can help with tracking long-term LUE. The activity of defining, building and applying models that represent functions and processes related to the dynamics of land use/land cover, population, employment and

transportation in urban areas is referred to as urban modeling usually embodied in computer programs (Batty 2009; Bhatta 2013). Since the 1950s, urban planners, geographers and ecologists have devised several urban models (Berling-Wolff and Wu 2004). Thus, many analytical and static urban modeling approaches that are based on diverse theories such as rank-size relationship, urban geometry, economic activities, city structures, etc. are also available in the literature. However, such models primarily deal with historical evolution, growth and expansion at the spatiotemporal dimension; these models cannot be applied to predict future urban growth.

In contemporary urban research, models of urban growth are often deployed to understand the nature of the spatiotemporal pattern of urban growth and to simulate future urban scenario, and these are helpful for future resource allocation and urban planning. Lambin (2004) summarized the land-use change model into four broad groups: (i) statistical models, (ii) stochastic models, (iii) optimization models and (iv) process-based dynamic simulation models. Pooyandeh et al. (2007) categorized urban growth models into two broad parts—(a) complexity models and (b) temporal GIS models. Besides, the complexity models are further subdivided into models based on cellular automata (CA), agent-based models, neural network-based models and fractal-based models. Batty (2009) recognized three broad categories of urban simulations: (a) land-use and transportation models, (b) urban dynamics models, and (c) CA, agent-based model and micro-simulation. In aggregate, commonly used models for simulating urban growth and land-use dynamics are categorized into four subcategories, namely empirical statistical, optimization, stochastic models and process-based dynamic simulation models (Lambin 2004; Zhang 2009).

A dynamic modeling system is preferred to understand the spatiotemporal of urban growth (Batty and Longley 1994). Considerable efforts have been made towards developing and improving dynamic urban modeling (Batty and Xie 1994; Landis 1995; Li and Yeh 2000; Batty 2005; Sahana et al. 2019). Significant improvement in the spatiality of urban growth came in 1980s only with the use of CA models. Since then, CA models have been widely used for modeling urban growth in a complex urban system (Xie 2010; Batty et al. 1999; Fang et al. 2005; Al-Ahmadi et al. 2009; Chowdhury and Maithani 2014; Mondal et al. 2017). Wu and Webster (1998) applied multi-criteria evaluation (MCE) transition rules to predict land-use conversion along the fringe areas of a rapidly growing metropolis. The domain experts, specifically in the field of modeling urban growth, use the CA model coupled with other techniques (Sahana, 2018) and machine learning approaches (e.g., Shafizadeh-Moghadam et al. 2021)—known as hybrid models. For a good discussion on integration of CA with machine learning approaches one may refer Shafizadeh-Moghadam et al. (2021). The cellular automata Markov (CA-MARKOV) is a widely employed such a hybrid model (Mondal et al. 2017; Olmedo and Mas 2018).

Over the years, researchers have developed and used different other sophisticated models to simulate and analyze urban growth, such as artificial neural network (ANN) (e.g., Almeida et al. 2008; Maithani 2009; Abiden et al. 2010; Shafizadeh-Moghadam et al. 2021), agent based model (e.g., Jjumba and Dragićević 2012; Arsanjani et al. 2013), genetic algorithm (GA) (Tang et al. 2007), geographically weighted regression (e.g., Mondal et al. 2015), SLEUTH model (e.g., Clarke et al. 1997; Herold et al. 2003; Jat et al. 2017), analytical hierarchy process (AHP) (e.g., Park et al. 2012; Devendran and Lakshmanan 2019), bivariate or stepwise multiple regression (e.g., Sudhira et al. 2004; Al-Sharif and Pradhan 2014), logistic regression (e.g., Hu and Lo 2007; Nong and Du 2011; Munshi et al. 2014; Dhali et al. 2019), Markov chain (MC) (e.g., Tang et al. 2007; Takada et al. 2010; Arsanjani et al. 2013) and fuzzy logic (e.g., Liu 2012). The multi-layer perceptron (MLP)

is a widely applied ANN approach in modeling and forecasting urban growth (Sharda 1994; Hu and Weng 2009; Mishra and Rai 2016; Sahana et al. 2018). In addition, the transition potential used in the MLP model is reported to be best performed as compared to other modeling techniques (Eastman et al. 2005). Some studies have used the MC in combination with ANN for modeling urban growth dynamics (e.g., Mondal et al. 2020). MC is believed to be a useful tool for modeling land use/land cover (LULC) change when the process of land cover change in an area is complex and challenging. The ANN modeling, in combination with MC, is capable of effective simulation of urban dynamics as ANN can fit complicated non-linear association between urban land use dynamics and factors driving urban growth (Eastman and Toledano 2018).

Urban expansion can efficiently be detected, mapped, monitored and analyzed using RS and GIS tools. Satellite imagery can present a synoptic view of a landscape at the frequent interval, provide images of areas inaccessible to conventional surveying, and reveal explicitly land use and land cover patterns, which is widely used as an input database to extract urban built-up areas. The technology of RS coupled with GIS is a cost-effective, technologically sound, useful and powerful tool, thus can be deployed to monitor and model urban growth dynamics. Since its inception in 1972, the time series Landsat data have been comprehensively used by researchers for change detection in spatiotemporal urban growth. With the advancement in research, researchers have devised different such models integrated with RS-GIS for quantifying and modeling the patterns and processes of urban expansion in cities (Mithun 2020; Mithun et al. 2021).

Recently, a number of research works have been devoted to comparing the suitability and performance of these models. Furthermore, various studies have also worked on spatial land consumption and the nature of SDG 11.3.1 (Schiavina et al. 2019; Wang et al. 2020; Jalilov et al. 2021). However, such urban growth modeling is very rare for the Indian cities, having a long history of urbanization. In the present day, Indian cities are the fastest-growing cities of the world that's why urban growth modeling is an almost need for sustainable urban planning. The present study assessed the spatiotemporal urban growth of Kolkata metropolitan area (KMA) during 1996–2016 and predicts the future urban growth using a comparative modeling framework. Further predicted growth model has been used to monitor urban land-use efficiency and sustainable urban development (SDG 11.3.1) in Kolkata metropolitan area (KMA). For this work, we have used three RS-GIS integrated techniques, namely Stochastic choice Markov chain (STCHOICE), CA-MARKOV, and MLP neural network (MLPNN) coupled with the multi-criteria evaluation (MCE) with the following objectives: (a) Identifying major driving factors or explanatory variables from the selected variables responsible for urban growth in KMA; (b) assessing the spatiotemporal urban growth of KMA during 1996–2016 using comparative modeling framework (c) Predicting future urban growth in KMA for the next two decades, i.e., for 2036, using the best modeling approach after successful validation and (d) Further, monitoring the SDG indicator 11.3.1 for sustainable urban development in KMA using the predicted maps.

2. The study area

Kolkata, erstwhile Calcutta, is a district and the capital of West Bengal, an Indian state. The city of Kolkata is about 300-year old and remained as India's capital till 1911 under British rule (Bhatta 2012). The present study considers the KMA (Figure 1) as the case study, which is the urban agglomeration of Kolkata city spreading either side of the Hooghly River along the north-south direction.
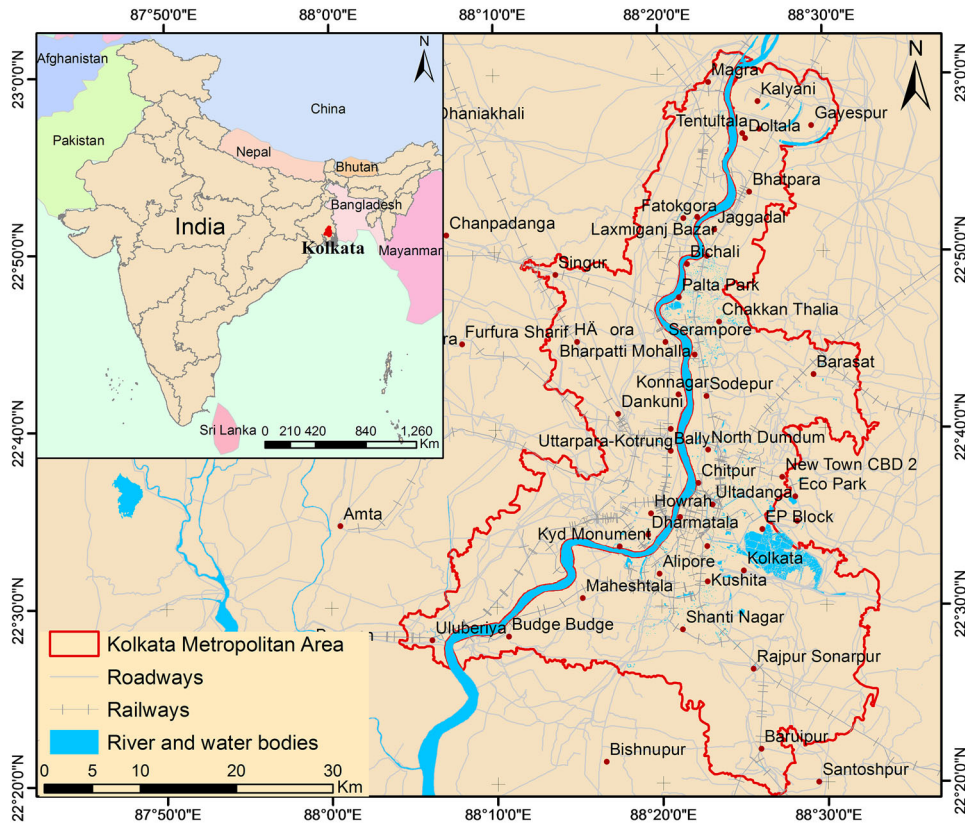
Figure 1. Location map of the Kolkata Metropolitan Area (KMA).

The KMA is the largest metropolitan area in West Bengal and after Mumbai and Delhi, the third most populous metropolitan area in India. It is the leading financial, commercial, educational, health, and research nucleus that cater to the requirements not only for the metropolitan but also for the entire state and Eastern India (KMDA 2011). Despite accounting for only roughly 18% of the state's population, the KMA's contribution to the state's economy is estimated around 30% of the gross domestic product. Kolkata and parts of West Bengal's other five districts, namely Haora, Hugli, North 24 Parganas, South 24 Parganas, and Nadia, make up the KMA (Mithun et al. 2016). Besides, the KMA comprises three municipal corporations, namely Kolkata municipal corporation (KMC) erstwhile Calcutta municipal corporation (CMC), Howrah municipal corporation, and Chandernagore municipal corporation, 39 municipalities, one cantonment, and parts of 24 community development (CD) blocks that contain *panchayat* (areas under a village council) areas. In aggregate, KMA comprises 72 cities, 572 towns, including Census towns[1] and villages (KMDA 2011; Mithun et al. 2016).

Under the British rule, the city of then Kolkata witnessed the active engagement of Calcutta Improvement Trust established in 1911 to assure the spatial planning in the form of construction new wide roads, channels for drainage, refurbishing an existing building and planning for the new neighborhoods (Ganesan, 2016; Rahaman et al. 2019). After independence, different organizations like Calcutta Metropolitan Planning Organization, KMC (formerly CMC), Kolkata Metropolitan Development Authority (KMDA) actively participated in the formulation and implementation of different spatial

Table 1. Details of the acquired database excluding satellite images.

Data type	Dataset (characteristic)	Year	Sources
SRTM Digital Elevation Model (DEM) 1 Arc-Second	Elevation (m), slope (°)	2014	USGS Earth Explorer
Landsat TM	Path & Row 138 & 44, 138 & 45 UTM (Zone 45N) & WGS 84	16.02.1996 and 12.12.2006	USGS Earth Explorer
Landsat OLI	Path & Row 138 & 44, 138 & 45 UTM (Zone 45N) & WGS 84	07.12.2016	USGS Earth Explorer
Socio-economic data	Population density	1991, 1996, 2001 and 2011	Census of India
	Commercial centers, major higher education institutes, urban centers, other urban amenities	1996–2011	Bureau of Applied Economics & Statistics, Govt. of West Bengal, SOI topographical maps, Google Earth satellite map
	Housing price	1996–2016	Directorate of Registration and Stamp Revenue, West Bengal, and Field survey
	Transport network, metro stations, railways, protected areas	1996–2011	SOI toposheet, Google satellite map, Open Street Map (OSM), and KMDA
Environmental data	Air quality index (AQI)	1996 and 2006	West Bengal pollution control board (WBPCB)

plans and policies in Kolkata. As a part of the spatial planning of Kolkata, Bidhannagar city was developed as a satellite town of Kolkata to accommodate the mushrooming population of the mother city between 1958 and 1965. After that in 1999 Newtown Kolkata city has been designed as a self-sustaining city to provide habitation to the high-income to low-income group of the city. For the proper development of Bidhannagar, New Town Kolkata Development Authority was formed in 2007. Presently along with KMDA and NKDA other government and quasi-government organizations like Housing & Urban Development Corporation Ltd., West Bengal and Housing Infrastructure Development Corporation Limited are actively participating in providing spatial infrastructure to assure the sustainable urban development of the KMA (KMDA 2011; Ganesan 2016; Mithun 2020).

3. Database and methodology

The present study used multispectral and temporal Landsat satellite imageries for 1996, 2006 and 2016 for the study area, that is, KMA obtained from the United States geological survey (USGS) Earth Explorer. The acquired images were geometrically corrected and almost free of cloud. Thermal bands of Landsat sensors were kept out of analysis owing to their coarser spatial resolutions compared to the optical bands. An administrative map of KMA was collected from the KMDA bearing administrative boundary at district, corporation, municipality, and community development (CD) block-level administrative boundary within the KMA. For modeling urban growth, a set of socio-economic and biophysical data such as river, metro network, railways, roads, river, presence of protected parks, etc., was collected from various sources (Table 1). The survey of India (SOI) topographical maps of old and open (new) series, Google earth map, reference map acquired from the national atlas and thematic mapping organization, India, and ground

control points collected by global positioning system survey were used for assessing the accuracy of the classified images. The corporation, municipality, and CD Block level population data were obtained from the Census of India's official website. The air quality-related data, that is, air quality index (AQI), was acquired from the official web portal of the West Bengal pollution control board (WBPCB). Besides, the literature survey and an experts' opinion survey consisting of planners, academicians, administrators, and local people were conducted to select and weigh factors for urban growth in KMA.

The study adopted the state-of-the-art SVM classifier for classifying the preprocessed (geometrically and radiometrically corrected) Landsat TM and Landsat OLI images (Table 1) in order to prepare the LULC maps for 1996, 2006 and 2016 (Mithun 2020; Mithun et al. 2021). In the present study, the LULC classification scheme was developed in tune to reflect the major land-use types of KMA. Some similar studies (e.g., Araya and Cabral 2010; Ahmed and Ahmed 2012; Shafizadeh-Moghadam and Helbich 2013) and an experts' opinion survey with planners and academicians were taken into account for the classification scheme. The approach of Anderson (1976) was also followed to define the undertaken LULC classes. The definition of present LULC classes is available in Mithun et al. (2021).

The whole classification process was executed in ArcGIS 10.6 (ESRI, 2017). Using all optical bands from Landsat TM and OLI data, the multiband raster data were prepared for all the respective years (1996, 2006 and 2016). The Training Sample Manager in ArcGIS was used to collect representative training samples for all the land cover classes from the multispectral raster data for each year. With 300 representative training samples per class, a sum of 1800 samples (for six land cover classes) was collected from the multispectral raster data for each year. The prepared original multiband images were used as an input dataset to train SVM classifier for each year separately. Also, the multispectral base images were used as ancillary data to generate attributes and other required information for classification. Then, the output classifier definition files were used in the Image Classifier tool in ArcGIS to produce LULC map for each year separately (Mithun 2020). The final LULC images of KMA for the years 1996, 2006 and 2016 were produced with six LULC classes, namely built-up, mixed built-up, water bodies, vegetation, agricultural land, and barren land. The LULC maps were used as input databases in modeling urban growth.

The methodology adopted for modeling urban growth in the present study applying the three modeling approaches, namely STCHOICE, CA-MARKOV, and MLPNN, is represented in Figure 2. The first box in Figure 2 presents collection, preprocessing, classification and accuracy assessment of SRS data to produce LULC maps of KMA for 1996, 2006 and 2016. Subsequently, the second, third and fourth boxes in Figure 2 depict stages of simulation of urban growth for the year 2016 in KMA applying STCHOICE, CA-MARKOV and MLPNN modeling approaches, respectively. The fourth box also presents the prediction of future urban growth in KMA for the year 2036 using the MLPNN approaches.

3.1. Stochastic-Markov chain (STCHOICE) model

The STCHOICE integrates stochastic processes with MC analysis. When the past trend of LULC dynamics is understood, it can be very useful. According to the Markovian process, the future urban expansion in a given area at time t_2 may be simulated from the immediate proceeding state, that is, at time t_1. The STCHOICE generates a future LULC map by evaluating and combining conditional probabilities that each LULC class exists at each
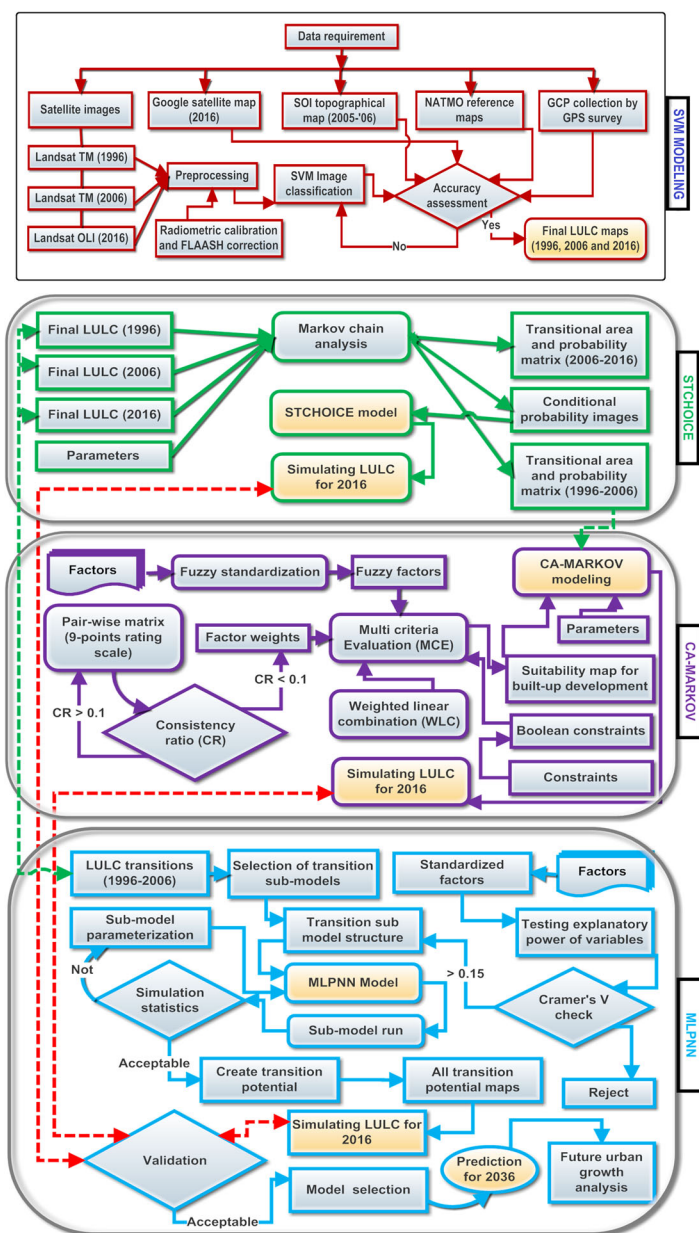
Figure 2. Methodological flowchart showing the implementation of modeling urban growth in a comparative framework.

pixel position against a rectilinear random probability (Ahmed and Ahmed 2012; Eastman 2015). The TerrSet (Eastman 2015) was employed for STCHOICE modeling in the present study, where the present LULC of KMA (2016) was simulated based on the LULCs of 1996 and 2006.

In MC analysis, the transition probability matrix expresses the probabilities related to the conversion from one state to another. Consider an MC process having n states S_1, $S_2 \ldots, S_n$ and P_{ij} denotes the probability corresponding to changing from state S_i to S_j as presented in Equation (1).

Table 2. A 5 × 5 contiguity filter used in CA-MARKOV modeling.

0	0	1	0	0
0	1	1	1	0
1	1	1	1	1
0	1	1	1	0
0	0	1	0	0

$$P\left(\ \xi_{t+1} = S_j|\ \xi_t = S_i\right) \tag{1}$$

Then the transition matrix is defined as in Equation (2),

$$P = \begin{vmatrix} p_{11} & \cdots & p_{1n} \\ \cdots & \cdots & \cdots \\ p_{n1} & \cdots & p_{nn} \end{vmatrix},\ p_{ij} \geq 0,\ \sum_{j=1}^{n} p_{ij} = 1,\ i = 1, \ldots, n \tag{2}$$

The forecasting of future LULC can be calculated following Equation (3) (Al-Sharif and Pradhan 2014),

$$S(t+1) = P_{ij}.S(t) \tag{3}$$

where P_{ij}= transition probability matrix, $S(t)$ represents the state of land cover at time t, and $S(t+1)$ is the state of land cover at a time $(t+1)$.

3.2. Cellular automata (CA) model

A CA can be characterized as a dynamic spatial system, according to Barredo et al. (2003), in which the state of any cell in an array is determined by the previous state of the cell and its surroundings based on specific criteria.

Let, $S_{x_{ij}}^t$ is the status of a cell x_{ij} at position i, j at time t. $S_{x_{ij}}^t$ belongs to a set of states in a lattice. Then, the cell's status at time $t+1$ can be expressed as $S_{x_{ij}}^{t+1}$, as in Equation (4) (Liu, 2008),

$$S_{x_{ij}}^{t+1} = f\left(S_{x_{ij}}^t,\ S_{\Omega_{x_{ij}}}^t\right) \tag{4}$$

where $\Omega_{x_{ij}}$ stands for a group of cells in the surrounding of the cell x_{ij}, and $S_{\Omega_{ij}}^t$ represents the states of the neighbor cells $\Omega_{x_{ij}}$, and f denotes a function that represents a set of transition rules.

Moreover, if the cell is regarded as a member of its immediate neighborhood, Equation (4) can be modified as Equation (5),

$$S_{x_{ij}}^{t+1} = f\left(S_{\Omega_{x_{ij}}}^t\right) \tag{5}$$

3.2.1. Cellular automata Markov (CA-MARKOV) model

In the present study, the CA-Markov module in TerrSet (Eastman 2015; Olmedo and Mas 2018) that integrates CA with MC was employed to model urban growth in KMA. The necessary inputs comprised a base land cover map, transition probability, and area matrix, suitability maps, and a user-defined contiguity filter. Using the model, the state of each LULC category at time t_2, that is, 2016 was determined based on the change in LULC class between time t_1 (1996) and t_0 (2006). Based on its neighbors, the CA-MARKOV used a spatially explicit contiguity filter to alter the state of cells, in predicting the future LULC in KMA for 2036. For this study, 5 × 5 contiguity filter was used, represented in Table 2.

3.2.2. The multi-criteria evaluation (MCE)

The present study performed an MCE for combining the selected factors (Table 5) that drive urban growth and constraints or resisting forces resisting urban growth in KMA. The previous studies (Park et al. 2011; Eastman 2015; Aburas et al. 2017) and an experts' opinion survey were taken into consideration for identifying the driving forces and constraints.

In the MCE module, the continuous factors were standardized into the desired range using fuzzy standardization applying sigmoidal, linear and J-shaped membership functions. It further allowed to use specific membership function shapes, such as monotonically increasing, monotonically decreasing, or symmetric, depending upon the nature of the factor under consideration (Eastman 2015).

Once the standardized images were created, the WEIGHT module in TerrSet (Eastman 2015) was used to derive relative weights of factors under consideration applying a pairwise comparison process under the AHP framework (Saaty 1977). Here, a 9-point reciprocal continuous scale was used to ascertain the relative importance of each factor in relation to all others. (Eastman et al. 1995, 1998). Assigning of relative weights to different factors was determined considering the literature review and the experts' opinion survey.

The consistency ratio (CR) was calculated in order to assess the degree of consistency in the weights so obtained (Eastman 2015), as in Equation (6),

$$CR = \frac{CI}{RI} \tag{6}$$

where $RI=$ Random Index, and $CI =$ the degree of consistency in weight assignment, which can be calculated using the formula in Equation (7),

$$CI = \frac{\pi_{\max}^{-n}}{n} \tag{7}$$

where $\pi_{\max}$ denotes the size of the principal eigenvalue in the decision matrix, and the number n denotes the size of the decision matrix. A CR of 0 denotes a perfect pairwise comparison, while a CR value higher than 0.10 indicates the presence of inconsistencies in the matrix.

Following the development of the criteria maps (factors and constraints), the MCE module in TerrSet was used to combine factors and constraints using weighted linear combination (WLC) to create a suitability surface. Eastman (1999, 2015) considered previous researches by Malczewski et al. (2003) and Behera et al. (2012).

Equation 8 illustrates the preparation of suitability map deploying WLC combination procedure (Eastman et al. 1998),

$$S = \sum w_i x_i \tag{8}$$

where $S =$ suitability, $w_i =$ weight of factor i and $x_i =$ criteria score of factor i. If Boolean constraints are incorporated, then the procedure can be modified, as in Equation (9) (Eastman et al. 1995, 1998; Eastman 2015),

$$S = \sum w_i x_i * \prod c_j \tag{9}$$

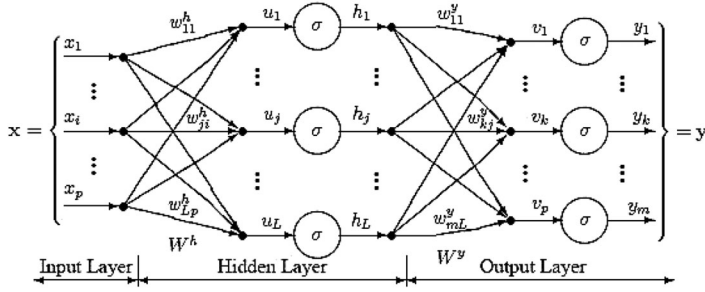where $c_j=$ criteria score (0/1) of constraint j and $\prod=$ product.

Figure 3. An MLPNN Model (Source: Ahmed 2011).

3.3. Multi-layer perceptron neural network (MLPNN) Markov model

An MLPNN (Figure 3) is a kind of feed-forward neural network in which one or more layers exist between input and output layers (Atkinson and Tatnall 1997; Ahmed and Ahmed 2012; Taud and Mas 2018).

MLPNN learning algorithm is a backward propagation (BP) algorithm that uses data from training sites (Ahmed and Ahmed 2012; Eastman 2015). The input that is received by a single node weighted as in Equation (10),

$$net_j = \sum \omega_{ij} O_i \tag{10}$$

where ω_{ij} represents weight difference between nodes i and j, and the output from node i is denoted by O_i.

The result (output) from a nod j is calculated, as in Equation (11),

$$O_j = f(net_j) \tag{11}$$

where f represents a non-linear sigmoid function used to derive the weighted sum before the information goes to the next layer.

The relation presented in Equation (11) is called forward propagation (FP). The output nodes' activities are compared to the expected activities for those nodes (Atkinson and Tatnall 1997; Eastman 2015). Thus, the error is transmitted backwards via the network, and network weights are adjusted, as in Equation (12),

$$\Delta\omega_{ij}(n+1) = \eta(\delta_j O_i) + \alpha\Delta\omega_{ij}(n) \tag{12}$$

where η denotes a parameter of learning rate; δ_j represents a measure of rate of change in error and α is the parameter of momentum.

The process of FP and BP is iterated until the errors of the network minimize to an acceptable level. The network is trained to provide appropriate weights for the network between the input and hidden layers, as well as the network between the hidden and output layers, in order to classify unknown pixels (Ahmed and Ahmed 2012; Eastman 2015). The numbers of hidden layer nodes are estimated using Equation (13),

$$N_h = INT\left(\sqrt{N_i \times N_o}\right) \tag{13}$$

where N_h denotes hidden nodes; N_i represents input nodes; and N_o indicates the output nodes.

Training accuracy is also affected by the quantity of training samples used. A too small sample size may not accurately represent the pattern of LULC class, while a too high may result in overlapping (Ahmed and Ahmed 2012). The root mean square error (RMSE) is used to determine an acceptable error rate, as presented in Equation (14),
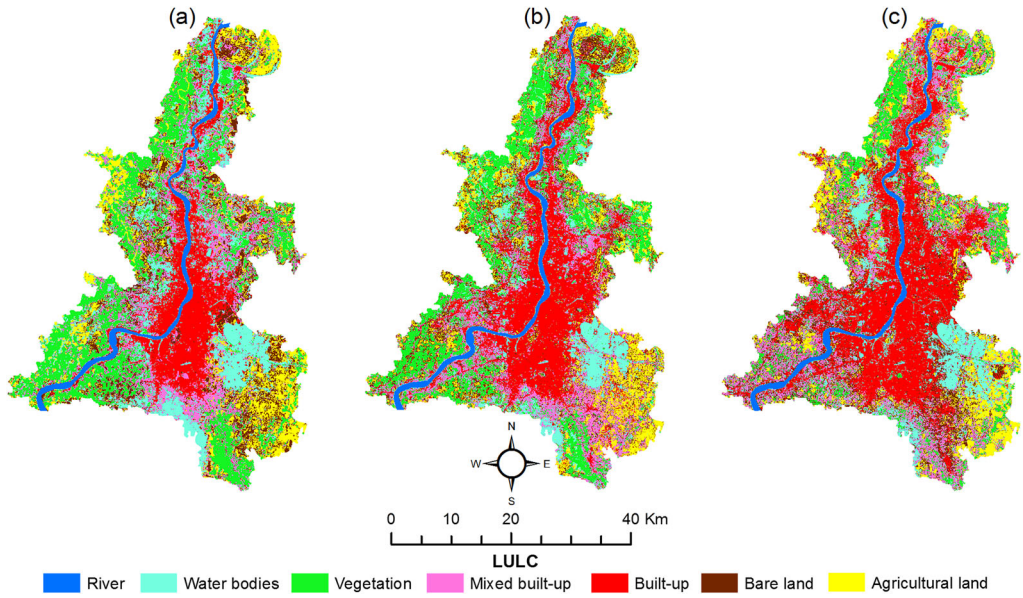
Figure 4. Classified LULC maps of KMA in 1996 (a), 2006 (b) and 2016 (c) (Mithun et al. 2021).

$$RMSE = \sum (e_i)^2 \Big/ N = \sum (t_i - a_i)^2 \Big/ N \tag{14}$$

where N denotes elements; i is element's index; e_i denotes error of the ith element; t_i is the target value and a_i is calculated value. The MLPNN modeling was implemented employing the 'Land Change Modeler' module in TerrSet (Eastman 2015).

4. Results

All three classified images of 1996, 2006 and 2016 depict six LULC classes, namely built-up, mixed built-up, water bodies, vegetation, agricultural land and barren land, as in Fig. 4. Overall classification accuracies were reported to be 89.75% in 1996, 92.00% in 2006, and 92.75% in 2016. The corresponding Kappa index of agreement was found at 0.879, 0.904 and 0.912, for 1996, 2006 and 2016, respectively. Thus, the levels of achieved accuracies obtained in the current study were satisfactory and acceptable (Mithun et al. 2021).

4.1. Results of STCHOICE modeling

Results of STCHOICE modeling are presented with the following heads.

4.1.1. Transition magnitude and probability into built-up and mixed built-up covers

The distribution of non-urban land covers that were subjected to transition into built-up and mixed built-up classes in the KMA during the period, that is, 1996 − 2016, is represented in Figure 5. During the period, a total of 49,111 ha non-built-up land areas were converted into built-up class. The land cover of vegetation dominates the process of conversion into built-up areas constituting around 36.74% out of total such transformation. This conversion is followed by water body (17.69%), bare land (17.63%), and agricultural land (15.19%) in order of magnitude. This illustrates that vegetal cover is the most vulnerable land cover to be transitioned into built-up cover in KMA. Besides, Figure 5(a) also
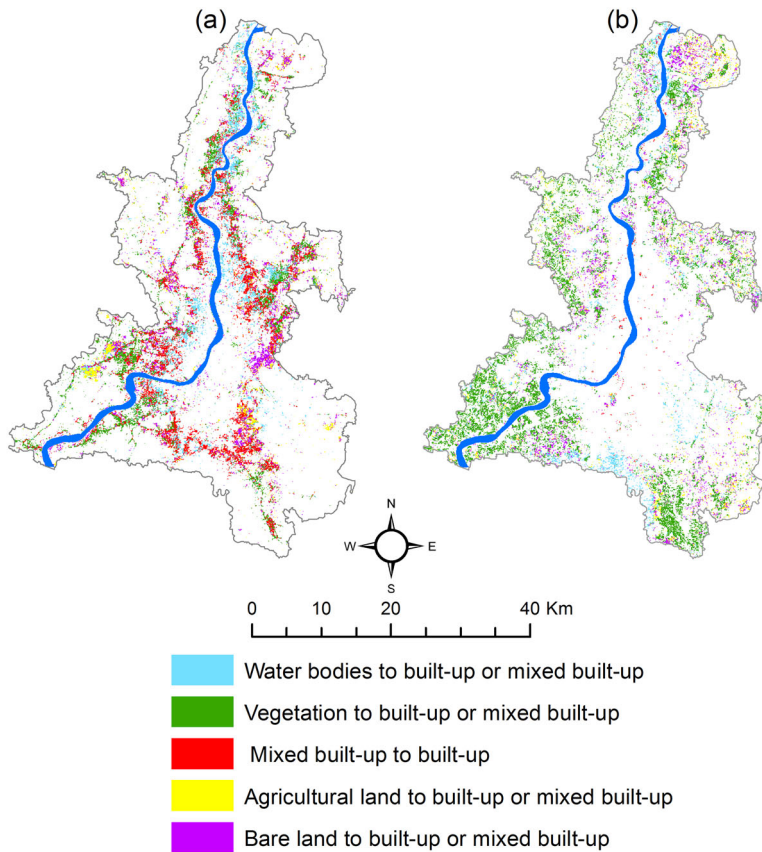
Figure 5. Spatial view of non-built-up covers that were transitioned into built-up and mixed built-up covers in KMA during 1996–2016; (a) transition of non-built-up covers into the built-up cover; and (b) transition of non-built-up covers into mixed built-up covers.

highlights that the mixed built-up class tops (30.87%) the process of transition into urban built-up areas followed by vegetation (21.35%), water bodies (20.74%), and bare land (17.31%), while agricultural land (9.74%) stands as least important to be converted into built-up covers as in Figure 5(a). This explains that the mixed built-up class is subject to switch into built-up areas with time in the metropolitan along the boundary of the built-up regions. On the other hand, as depicted by Figure 5(b), the transition into mixed built-up is dominated by the vegetal cover (53.67%) lying at the periphery of urban built-up cover followed by bare land (17.97%), and agricultural land (12.79%).

As discussed earlier, the STCHOICE combines both stochastic processes and MC analysis. Applying MC analysis, the LULC of KMA was modeled for 2016 based on the land cover transition during the previous ten years, that is, 1996 to 2006. The MC analysis produced a transition area matrix, a transition probability matrix, and a set of conditional probability images for the change in 2016 by analyzing two qualitative land cover images for two different years, that is, 1996 and 2006 (Table 3).

The transition probability matrix, as in Table 3, depicts the probability that each land cover would change to other land covers in 2016. The diagonal elements of the matrix hold higher probabilities as they indicate an intra-type land cover transition, that is, self-replacement referring to land cover types that remain similar, while off-diagonal elements show probabilities of inter-type land cover transitions. The corresponding number of

Table 3. Markovian transition probability matrix presenting the probability of each land cover to change into other land covers during 2006–2016 based on the trend during 1996–2006.

LULCs	Water bodies	Vegetation	Mixed built-up	Built-up	Agricultural land	Bare land
Water bodies	0.3725	0.1290	0.1076	0.1254	0.1326	0.1329
Vegetation	0.1083	0.4995	0.1664	0.0261	0.0875	0.1122
Mixed built-up	0.0000	0.0000	0.3553	0.6447	0.0000	0.0000
Built-up	0.0015	0.0000	0.1615	0.8368	0.0002	0.0001
Agricultural land	0.1422	0.0930	0.0240	0.0256	0.4401	0.2751
Bare land	0.1137	0.1433	0.0472	0.0588	0.3807	0.2562

pixels that would be transitioned from each land cover to other different land covers is presented in Figure 6. Both the tables highlight that all the non-built-up land cover shows a high degree of transition to be transformed into built-up and mixed built-up classes.

4.1.2. Conditional probability images

The MC analysis produced a set of conditional probabilities images based on the conditional probability matrix (Figure 6). They are called so as the probabilities are conditional to the current state. The images are projected for the future ten years to 2016 from the two previous land cover images of 1996 and 2006, depending upon the past trend of land cover transformation during the last ten years, that is, during 1996–2006. The images show the level of probability of being a particular land cover in 2016. The Markovian probability image of being built-up areas, as in Figure 6(d), ranges up to 0.84 as highest among the land covers with higher values towards central parts of the metropolitan, whereas the probability being the mixed built-up areas ranges up to 0.36 with higher values along with the areas lying outside of mixed built-up cover as in Figure 6(c). Therefore, a large-scale further built-up expansion would occur in 2016 in the metropolitan with being built-up at the central part and mixed built-up at the peripheral part at the cost of other non-built-up covers.

4.1.3. Simulating urban growth for 2016

Based on the Markovian conditional probability images, the land cover map of KMA was predicted for 2016, deploying a stochastic choice decision model through evaluating and aggregating conditional probabilities. This model was implemented in TerrSet (Eastman 2015), a widely used RS and GIS-based platform. This simulation is based on the past ten years of land cover transition, that is, 1996–2006, performed by MC analysis. The predicted original image is represented in Figure 7(a), which looks quite pock-marked. Besides, a 3 × 3 mode filter was applied to the original simulated image that resulted in the generation of a much clear predicted image, as presented in Figure 7(b).

4.2. Results of the CA-MARKOV modeling

As discussed before, the CA-MARKOV modeling was implemented employing CA-Markov module in TerrSet (Eastman 2015) combining MC, CA and MCE. The results on the CA-MARKOV Modeling are as follows.

4.2.1. MC based transition of areas

The MC analysis-based category-wise statement of areas under each land cover that went into transition during 1996–2006 is presented in Table 4, which was required for the implementation of CA-MARKOV modeling. Table 4 also highlights that all the non-built-
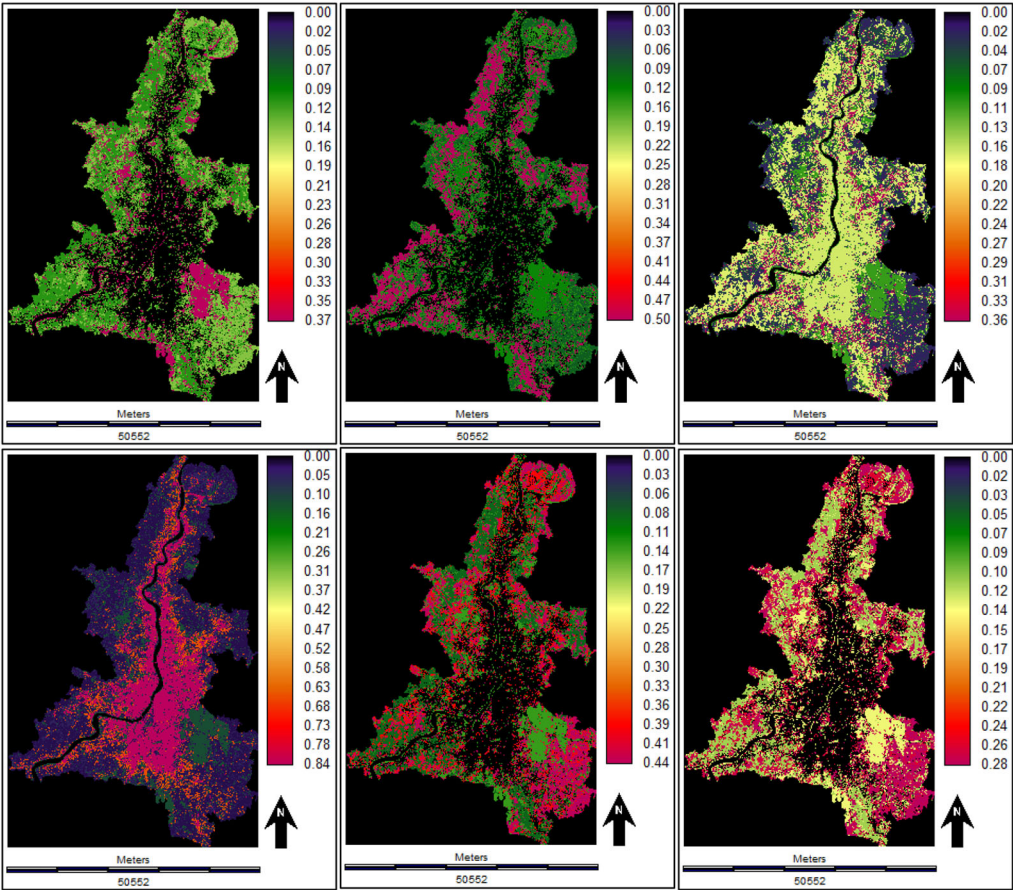
Figure 6. Markovian conditional probability images for being the land covers in 2016 based upon the past trend of land cover transition during 1996–2006; (a) being water bodies, (b) being vegetation, (c) being mixed built-up, (d) being built-up, (e) being agricultural land, and (f) being bare land.

up land covers show higher magnitude (in terms of number of pixels) of transition into built-up and mixed built-up areas in KMA.

4.2.2. Standardization of factors and constraints

In the present study, the built-up suitability map was prepared involving an MCE. The MCE combined the selected factors or explanatory variables that drive urban growth and constraints or resisting forces that resist urban growth in KMA. Table 5 represents major groups of factors, namely physical, socio-economic, linear infrastructures, and environmental factors identified in this study. All the considered factors were standardized by fuzzy standardization on a byte scale 0–255 with 0, indicating least while 255 indicating most suitable for the objective under consideration (Figure 8). A pixel within a built-up land cover has the highest suitability, which decreases with distance, and a pixel near to built-up areas has maximum like to be converted into built-up cover.

Table 5 also reflects the types and shapes of fuzzy membership function, and the position of inflection points used for factor standardization. Three types of fuzzy membership, viz., monotonically decreasing sigmoid, J-shaped, and linear functions were used in the present research in agreement with the research of Araya and Cabral (2010) and
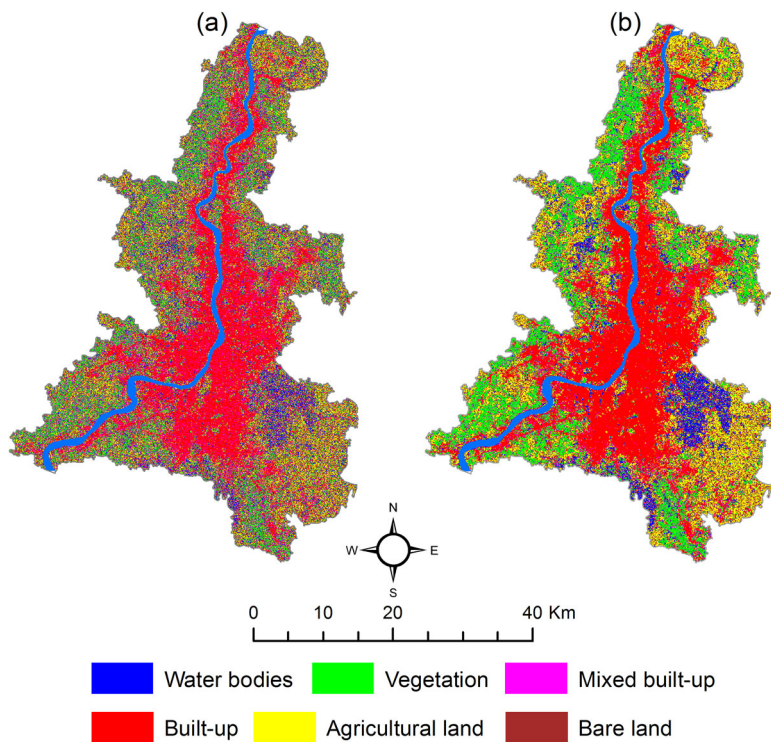
Figure 7. The STCHOICE simulated land cover map of KMA for 2016 based on Markovian conditional probability images of 1996–2006; (a) original predicted image of 2016; and (b) 3 × 3 mode filter generated predicted image of 2016.

**Table 4.** Matrix of pixel numbers transitioned to different land covers during 1996–2006.

LULCs	Water bodies	Vegetation	Mixed built-up	Built-up	Agricultural land	Bare land
Water bodies	100218	34702	28954	33746	35688	35757
Vegetation	44393	204668	68161	10694	35860	45966
Mixed built-up	0	0	64679	117344	0	0
Built-up	601	0	66272	343475	81	49
Agricultural land	53317	34890	9012	9589	165064	103192
Bare land	30581	38554	12708	15820	102429	68933

Mondal et al. (2017) with adjustable settings (Table 5) for standardization of the factors. However, for the majority of the factors used J-shaped standardization type explaining that the factors were produced based on Euclidean distance. The position of inflection points explains the nature of the function changing with distance. In case of J-shape function for the distance from the major roads explains that the areas within 200 m of the primary roads are highly suitable for built-up development (Table 5). The suitability decreases rapidly with distance up to 1000 m; however, it never reaches zero. On the other hand, the linear membership function seems to be suitable for factors like distance from existing developed areas. Because of the agglomeration effect, areas nearer to built-up areas transform into built-up areas faster than remote areas. It explains that suitability regularly decreases with an increase in distance.

Thus, the factors expressed a varying degree of relative suitability for the decision under consideration (Figure 8), while constraints are always Boolean. In this study, such

Table 5. The undertaken factors and fuzzy standardization parameters for CA-MARKOV modeling.

Factors	Membership function types	Membership function shape	Control points
Distance from built-up areas	Linear	Monotonically decreasing	200–2000 m
Distance from major roads	J-shaped	Monotonically decreasing	200–1000 m
Minor road distance	J-shaped	Monotonically decreasing	50–200 m
Nearest town/city distance	Linear	Monotonically decreasing	500–5500 m
Distance from railways	J-shaped	Monotonically decreasing	200–1000 m
Distance from metro	J-shaped	Monotonically decreasing	200–2000 m
Distance from major bus stands	J-shaped	Monotonically decreasing	100–500 m
Distance from commercial centers	Linear	Monotonically decreasing	0-6000 m
Distance from industries	J-shaped	Symmetric	0–100–500–5000 m
Slope	Sigmoidal	Monotonically decreasing	0°–10°
Elevation	Sigmoidal	Monotonically decreasing	4–20 m
Population density	Linear	Monotonically decreasing	920–10000 p/sq.km
Housing cost	Linear	Monotonically decreasing	Rs. 1500–6000
Air quality index (AQI)	Linear	Monotonically decreasing	87–120
Land use likelihood	Linear	Monotonically decreasing	–
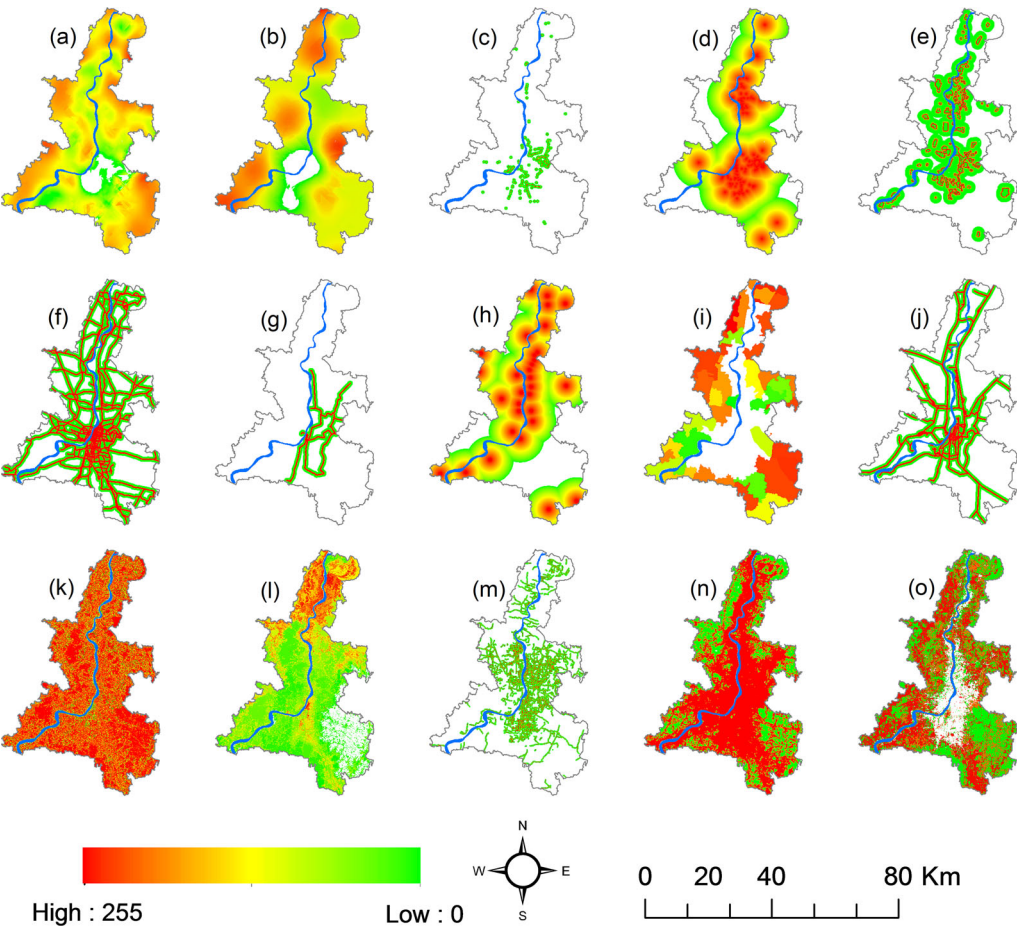
Figure 8. Fuzzy standardized byte scale (0–255) factors used in MCE in order to prepare suitability surface for built-up development. The fuzzy factors include (a) housing cost, (b) air quality index, (c) distance from major bus stands, (d) distance from commercial centers, (e) distance from industries, (f) major road distance, (g) distance from metro, (h) nearest city distance, (i) population density, (j) railway distance, (k) slope, (l) elevation (DEM based), (m) minor road distance, and (n) distance from built-up or developed areas and (o) land use likelihood.

Table 6. The pairwise comparison matrix (Saaty 1977) for the derivation of factor weights based on a 9-point rating scale where each factor is compared with every other factor for its relative importance.

		1	2	3	4	5	6	7	8	9	10	11	12	13	14	15
								Factors*								
1	F	1														
2	A	1/5	1													
3	C	3	5	1												
4	T	3	5	1	1											
5	O	1/3	3	1/3	1/3	1										
6	R	5	7	5	7	5	1									
7	S*	3	7	3	3	3	1/3	1								
8		1/5	3	1/5	1/3	1/5	1/7	1/7	1							
9		3	9	1	1	3	1	1	5	1						
10		5	7	3	3	3	1/3	3	3	3	1					
11		5	7	1	1	1	1/3	1/5	5	1	1/3	1				
12		1/3	1/3	1/5	1/5	1/5	1/7	1/7	1/3	1/5	1/5	1/3	1			
13		1/5	1/3	1/7	1/5	1/5	1/9	1/9	1/3	1/9	1/7	1/7	1/7	1		
14		1/3	1/3	1/5	1/5	1/5	1/7	1/5	1/3	1/5	1/5	1/5	1/3	3	1	
15		5	7	5	5	7	5	5	7	7	7	7	9	9	7	1

*1 = Housing cost, 2 = air quality index, 3 = distance major bus stands, 4 = distance from commercial centers, 5 = distance from industries, 6 = distance from metro, 7 = nearest city distance, 8 = population density, 9 = major road distance, 10 = land use likelihood, 11 = railway distance, 12 = slope, 13 = elevation, 14 = minor road distance, and 15 = distance from built-up or developed areas.

Boolean constraints maps of rivers, wetlands and parks were used in MCE while generating suitable surfaces for built-up development.

4.2.3. Factor weights

The relative weights of factors under consideration developed based on the pairwise comparison matrix under an AHP framework are represented in Table 6. Using a 9-point reciprocal continuous scale, each factor was scored for its relevance relative to every other factor in relation to the suitability of pixels for the activity being examined (Eastman et al. 1995; Eastman 2015). The relative importance of each factor was determined considering the literature and the experts' opinion survey (e.g., Araya and Cabral 2010).

The details of the weights of the factors determined in such a way are presented in Table 7. The obtained CR value in the present study was less than 0.1 which confirms the consistency of the defined weight schema, signifying that the factors with higher weights are statistically more significant for the objective under consideration.

4.2.4. Built-up suitability surface and simulation of urban growth for 2016

The suitability map, thus, prepared through MCE in the present study, is presented in Figure 9. The present study adopted the WLC procedure for aggregating all standardized factors and constraints utilizing a weighted average. This suitability map displays the degree of relative suitability for built-up development in the spatial dimension in KMA. A higher pixel value in the suitability map represents a higher degree of suitability for built-up development (Figure 9). The 'CA_Markov' module in TerrSet (Eastman 2015) was employed using the Markovian transition area matrix and built-up suitability image to simulate a LULC map of KMA for the year 2016 (Figure 10). In addition, a 3 × 3 contiguity filter was applied, and as discussed earlier, the land cover image of 2006 of KMA was taken as the base land cover in the CA-MARKOV simulation.

Table 7. Factor weights derived based on pairwise comparison procedure under the AHP framework.

Factors	Derived weights
Housing cost	0.0359
Air quality index	0.0161
Distance major bus stands	0.0545
Distance from commercial centers	0.0532
Distance from industries	0.0368
Metro distance	0.1487
Nearest town or city distance	0.0942
Population density	0.0213
Major road distance	0.0713
Land use likelihood	0.1063
Railway distance	0.0565
Slope	0.0164
Elevation	0.0085
Minor road distance	0.0127
Distance from built-up or developed area	0.2676
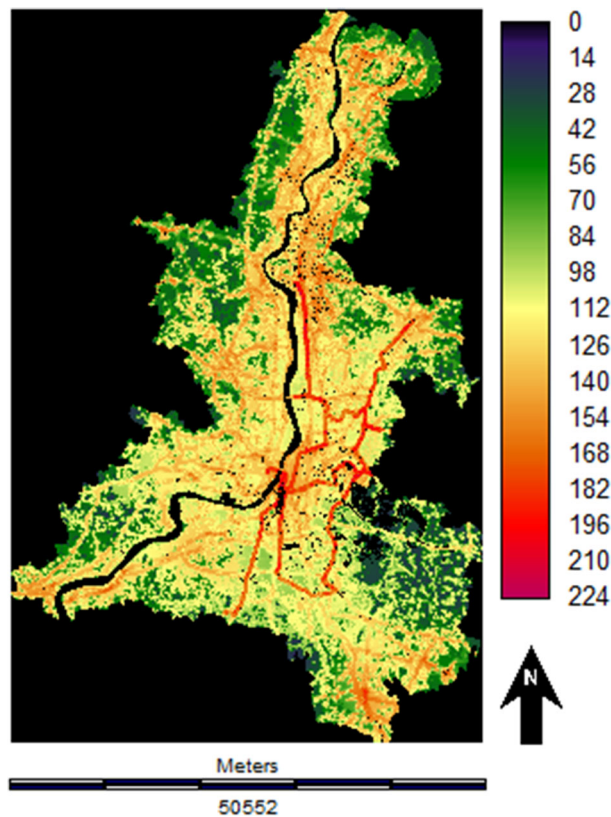
Figure 9. Suitability surface for built-up development in KMA for the year 2016.

4.3. Results of the MLPNN Markov modeling

The MLPNN model integrated with MC was implemented employing the 'Land Change Modeler' module in TerrSet (Eastman 2015). The results of the MLPNN modeling the presented with the following heads,
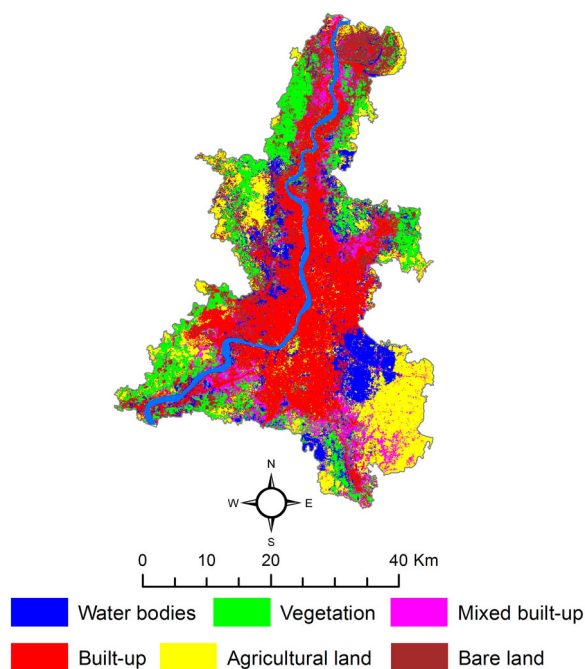
Figure 10. The CA-MARKOV simulated land cover map of KMA for 2016.

4.3.1. Transition sub-models

The non-built-up land covers are subjected to be transformed into mixed built-up and built-up with time in the metropolitan of KMA, as observed in the present research. Hence, the non-built-up land covers are primary contributors to increase built-up areas in KMA. Besides, the mixed built-up land cover is also subject to conversion into pure urban built-up areas with time. Therefore, the transitions by which non-built-up areas are being converted into mixed-built-up and built-up areas in the metropolitan were considered in the MLPNN modeling. Thus, a sum of nine transition sub-models was identified and considered to simulate the urban growth of KMA. The sub-models so selected include the transitions (1) from water bodies to mixed built-up, (2) from vegetation to mixed built-up, (3) from agricultural land to mixed built-up, (4) from barren land to mixed built-up, (5) from water bodies to built-up, (6) from vegetation to built-up, (7) from mixed built-up to built-up, (8) from agricultural land to built-up and (9) from barren land to built-up land cover. The first four transition sub-models explain the changing to mixed built-up covers, while the last five sub-models explain changing to built-up land covers within the metropolitan with respect to time (Figure 11). The undertaken sub-models considered land cover transitions during the period 1996–2006 as a training period.

4.3.2. Explanatory variables for the sub-model structures

The explanatory variables for modeling the transition sub-models under consideration were taken into account after a rigorous literature review and based on the experts' opinion survey and literature review. The explanatory variables are given in Table 8, whereas the variables normalized in a byte 0–255 scale are presented in Figure 12. The variables added to the model were characterized as dynamic or static (Eastman 2015) based on their roles in the urban growth of KMA they play. As such, all proximity variables such
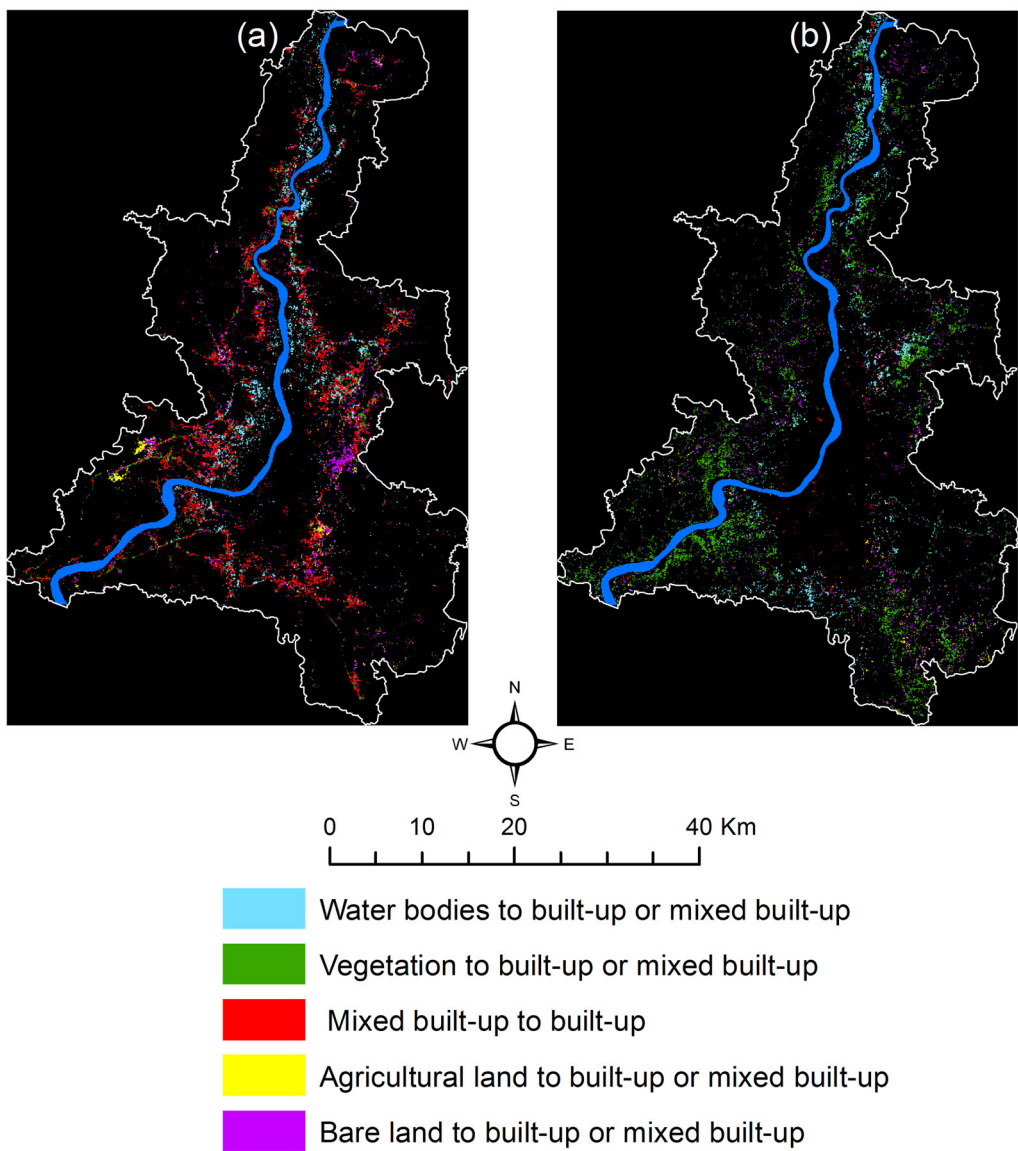
Figure 11. The transitions of other non-built-up LULCs into built-up and mixed built-up covers during 1996–2006; (a) transition of non-built-up covers into the built-up cover; and (b) transition of non-built-up covers into mixed built-up covers.

as distance to nearby town or city, metro distance, road distance, etc. were characterized as dynamic variables, while the variables such as slope, elevation, etc. were characterized as static variables. The quantitative measure of the variables was carefully tested, applying the Cramer's V values (Eastman 2015; Mondal et al. 2019) for all transition sub-models under consideration. As the sample sizes in the sub-models were large, all the corresponding p-values for the Cramer's V values were found to be close to 0, expressing that all pixels of the variables were sampled independently and were free of spatial dependence in their values.

Table 8. Nature and types of explanatory variables used in modeling of the undertaken transition sub-models.

Variables	Type	Unit
Built-up and mixed built-up distance	Land cover distance	Euclidean distance
Built-up and mixed built-up likelihood	Land cover likelihood	Relative frequency of pixels
Primary, secondary, and tertiary road distances; distance from metro, railways, railway stations, and major bus stations.	Transport network distance	Euclidean distance
Population density	Socio-economic data	Persons per sq. km
Commercial distance, distance from major higher education institute, a nearby town or city distance, distance from other urban amenities	Socio-economic and attribute distance	Euclidean distance
Air quality index (AQI)	Environmental features	–
Housing price	Socio-economic attribute	Rs./sq.ft
Slope	Topographic (physical) variables	Degree (°)
Elevation from mean sea level	Topographic (physical) variables	Meters (m)

### 4.3.3. Simulation performance of the MLPNN transition sub-models

The inclusion of all explanatory variables with satisfactory Cramer's V values was followed by simulation of the transition sub-models. For training and validation, simulation of the MLPNN sub-models required the sample pixels that were transitioned between the previous two land covers of 1996 and 2006. In the present study, during 1996–2006, the minimum number of pixels that transitioned from non-built-up to mixed built-up and from non-built-up or mixed built-up to built-up was found to be higher than 10,000 in eight cases out of the total nine sub-models (Table 9). Therefore, the maximum sample size was set at 10,000 in which 5000 pixels were used for training, and the remaining 5000 sample pixels were used for validation purposes. Besides, 10,000 iterations were fixed as simulation-stopping criteria along with RMS at 0.01 and accuracy at 100%.

In this research, the two parameters were set in automatic mode. With its default parameters, the MLPNN could adjust its learning rate automatically. The training and testing RMS graphs were achieved as smooth descents and almost overlapped to each other at the end of the simulation in all of the cases. The MLPNN provided accuracy and skill measures at the end of the simulation. In all nine transition sub-models, the achieved calibration accuracy level was found to be more than 90%, which is regarded as acceptable for further use. The skill measure (Eastman 2015) is simply a difference between observed accuracy and accuracy expected by chance varying from −1 to +1. In this research, the achieved skill measure was found to be close to +1 in all cases (Table 9). After achieving satisfactory statistics during both of the simulations, transition potential maps were created for all the nine transitions. Figure 13 depicts transition potential maps (1996–2006) showing changes from non-built-up to mixed built-up cover, while Figure 14 presents transition potential maps (1996–2006) reflecting transitions from non-built-up and mixed built-up to built-up cover. These maps show fuzzy set sigmoid function applied values ranging from 0 to 1, in which higher the value represents a greater degree of membership for that corresponding LULC type.

4.3.4. Simulating urban growth for 2016

Successful simulation of the nine transition sub-models was followed by the simulation of present urban growth in the metropolitan. For the purpose, an MC analysis was again
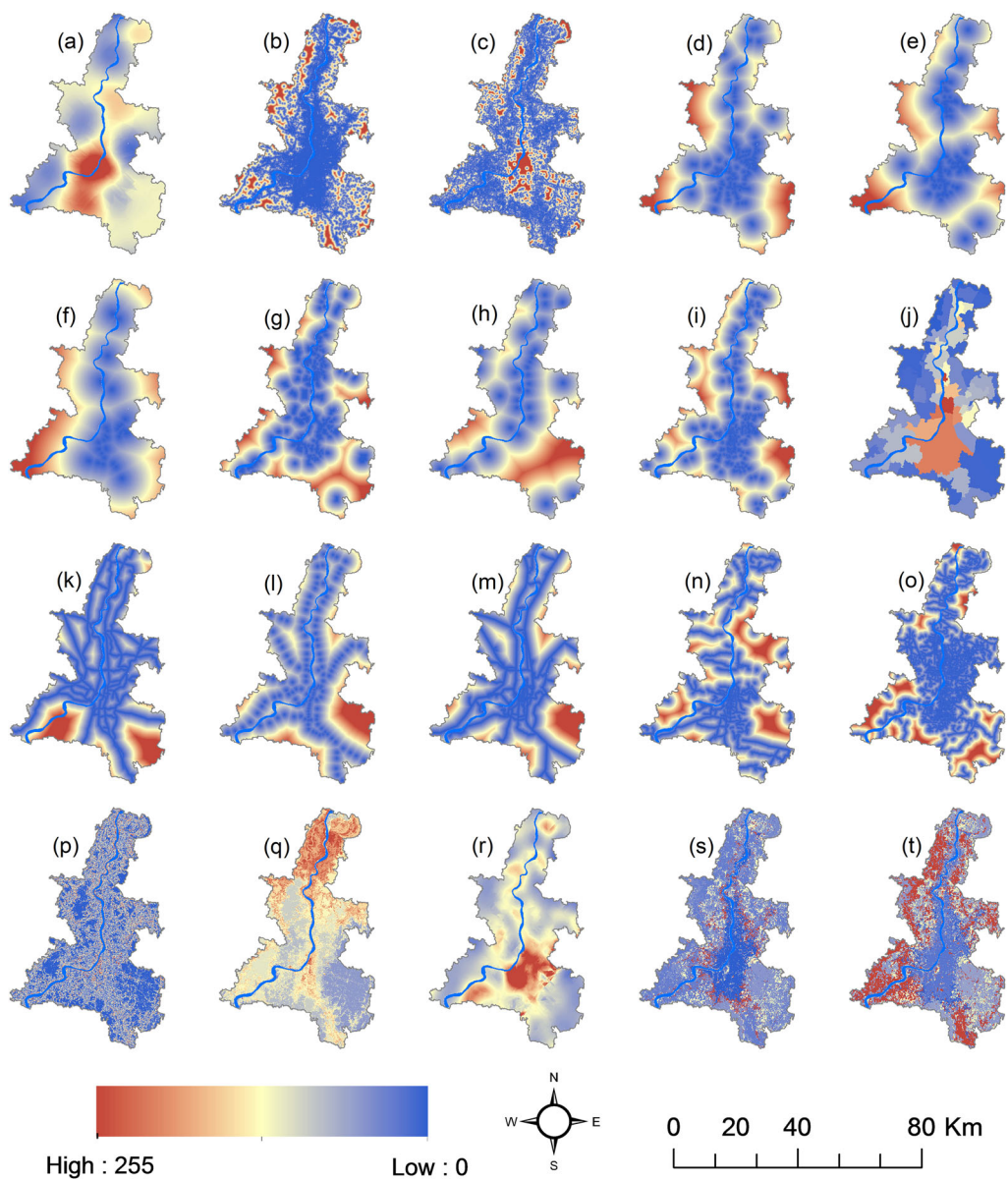
Figure 12. The explanatory variables used in MLPNN modeling normalized in a byte 0–255 scale; (a) air quality index, (b) distance urban built-up, (c) urban mixed built-up distance, (d) distance from major bus stops, (e) commercial distance, (f) distance from major higher educations, (g) industrial distance, (h) nearby town or city distance, (i) other urban amenities distance, (j) population density, (k) primary road distance, (l) railway station distance, (m) distance from rail lines, (n) secondary road distance, (o) tertiary road distance, (p) slope, (q) elevation, (r) housing cost or apartment price, (s) empirical likelihood of changing into built-up, and (t) empirical likelihood of changing into mixed built-up land cover during 1996–2006.

integrated with the MLPNN modeling to simulate urban growth in KMA for the year 2016. Accordingly, as per the change in demand, future predictions could be implemented, in which the future would be multiples of the training period. Figure 15 presents the MLPNN and MC simulated land cover map of KMA for 2016.

**Table 9.** Summary of simulation performance for the nine transition sub-models using MLPNN modeling.

Transition sub-model	Sample size (pixels)	Model accuracy rate (%)	Skill measure	Training RMS	Testing RMS	Most influential variable	Least influential variable
Agriculture to built-up	7672	96.98	0.9396	0.1689	0.1682	Distance from built-up surface	Distance from metro
Agriculture to mixed built-up	10000	96.20	0.9240	0.1940	0.1937	Distance from mixed built-up surface	Commercial distance
Bare land to built-up	10000	92.90	0.8581	0.2372	0.2421	Distance from built-up surface	Commercial distance
Bare land to mixed built-up	10000	92.76	0.8553	0.2500	0.2495	Distance from mixed built-up surface	Distance from metro
Mixed built-up to built-up	10000	89.21	0.7842	0.3080	0.3067	Distance from built-up surface	Population density
Vegetation to built-up	10000	98.51	0.9701	0.1263	0.1257	Distance from built-up surface	Primary road distance
Vegetation to mixed built-up	10000	93.01	0.8602	0.2361	0.2384	Distance from mixed built-up surface	Nearby town or city distance
Water bodies to built-up	10000	97.23	0.9447	0.1460	0.1497	Distance from built-up surface	Railways distance
Water bodies to mixed built-up	10000	96.69	0.9339	0.1515	0.1512	Distance from mixed built-up surface	Distance from metro

4.4. Model Validation

In the present study, to validate the results of simulation by the three modeling approaches the three simulated LULC maps (Figure 16) of KMA (2016) were compared with that of the actual LULC map of 2016 (Pontius 2000; Ahmed and Ahmed 2012). It shows that the MLPNN-simulated map closely approximates the actual land covers of KMA (Figure 16c). However, the STCHOICE and CA-MARKOV simulated maps deviate from the actual scenario to a large extent as compared to the one generated by the MLPNN approach. The present study employed three approaches for model evaluation: (a) per category wise percentage of correct prediction (PCP), (b) Kappa statistics and components of agreement and disagreement and (c) through building confusion matrices. However, many other updated techniques of model evaluation (e.g., Shafizadeh-Moghadam et al. 2021) have been used by different researchers discussion on which is outside of the scope of present study.

Table 10 presents class-wise comparison in the PCP in areas (ha) under different land covers with their prediction deviation (%) between actual and simulated maps of KMA. Less deviation in the areas illustrates more consistency in prediction, signifying the simulation as robust and vice versa. The STCHOICE model performed well in the predictions of bare land and water bodies as compared to other classes. The performance of CA-MARKOV was found satisfactory in the cases of bare land, water bodies, and built-up covers, depicting the magnitude of deviation less than ± 2%, whereas the MLPNN performed adequately in the simulation of all land cover classes. The results under the MLPNN show the magnitude of error less than or around ± 2% for all the six categories
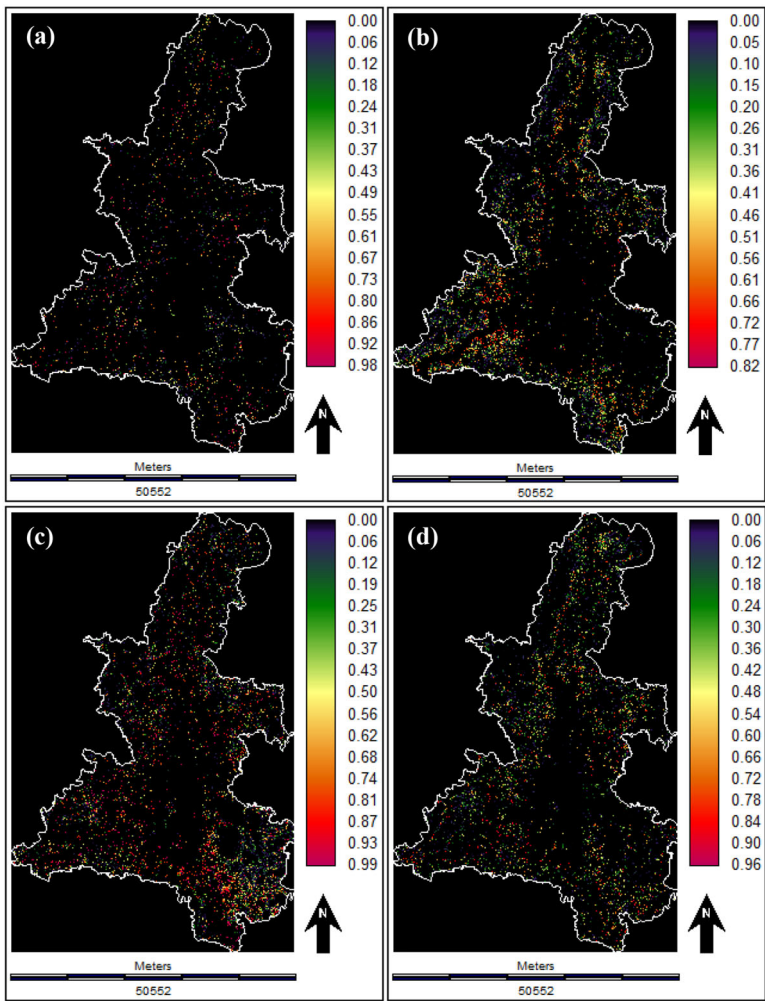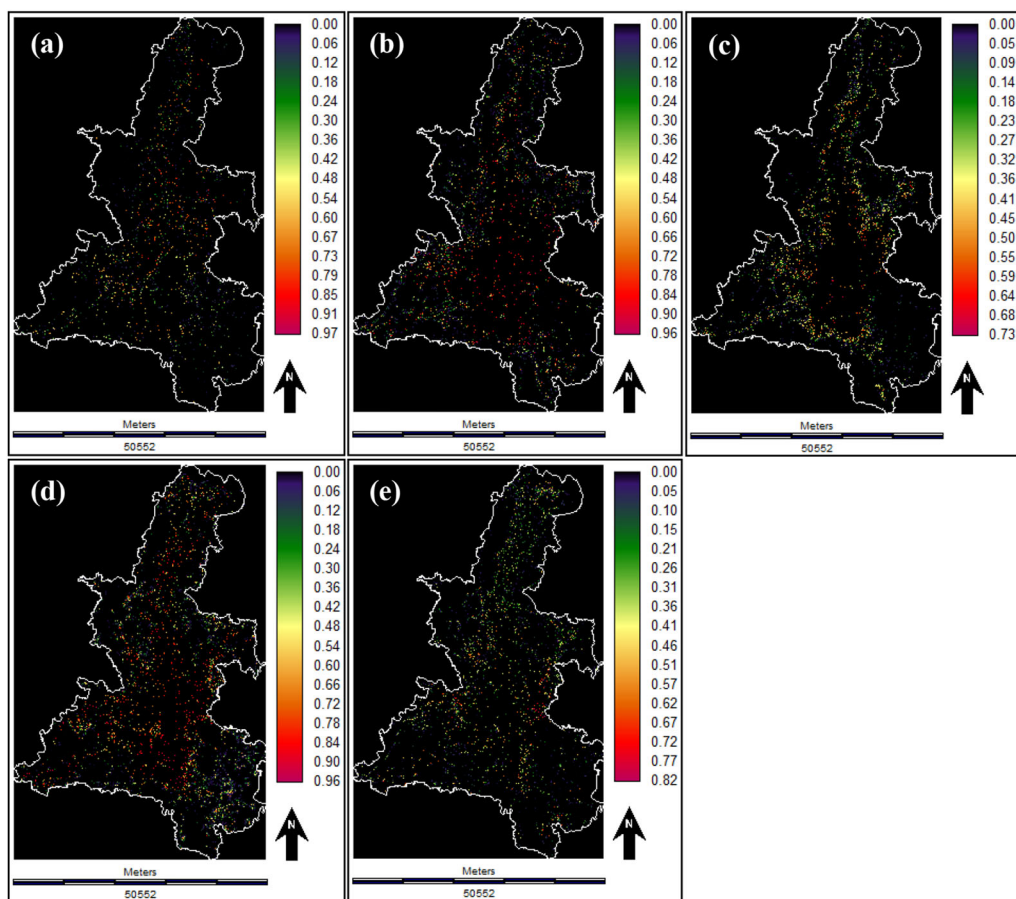
Figure 13. The MLPNN generated the potential for the transition from non-built-up land covers to mixed built-up cover during 1996–2006; (a) potential for the transition from water bodies to mixed built-up; (b) potential for the transition from vegetation to mixed built-up; (c) potential for the transition from agricultural land to mixed built-up; and (d) potential for the transition from barren land to mixed built-up land cover.

(Table 10). In addition, although the performance of CA-MARKOV is adequate in the case of built-up cover, the land cover of mixed built-up is overestimated by a $+8.25\%$; whereas, the MLPNN predicted built-up and mixed built-up land covers with a marginal error of about $\pm\,2\%$. Thus, the margin of prediction error is found to be minimum for the MLPNN modeling; hence, the performance of MLPNN simulation, as depicted by Table 10, is reasonably better as compared to the results of STCHOICE and CA-MARKOV modeling.

Table 11 presents Kappa statistics and components of agreement and disagreement relating to assessing the accuracy and validation of the simulated maps of KMA for 2016. The Kappa index of agreement, that is, $K_{standard}$ is observed at 0.54, 0.69 and 0.90 for the STCHOICE, CA-MARKOV and MLPNN simulations, respectively. Thus, the level of agreement achieved in the MLPNN simulation can be called as 'perfect,' while it is 'moderate' and 'substantial' for the STCHOICE and CA-MARKOV simulations,

**Figure 14.** The MLPNN generated potential for transition from other non-built-up land covers to built-up cover during 1996–2006; (a) potential for transition from water bodies to built-up; (b) potential for transition from vegetation to mixed built-up; (c) potential for transition from mixed built-up to built-up; (d) potential for transition from agricultural land to built-up; and (d) potential for transition from barren land to built-up land cover.

respectively (Table 11). The cell-by-cell visual comparison of the $K_{standard}$ between the actual and simulated scenarios for the three models and also reflects a similar trend spatially as represented in Figure 17. Apart from the $K_{standard}$, all other measures of the agreement under the Kappa family also feature relatively higher values for the MLPNN simulation. Moreover, the levels of total agreement and disagreement are found to be the highest and lowest, respectively, in the case of the MLPNN simulation (Table 11).

Further, the accuracy of the simulated LULC maps of 2016 produced by the three modeling approaches was assessed by building corresponding confusion matrices for the three simulated maps, after comparing the simulated maps with the actual LULC map of 2016. The results of overall accuracies were found at 61.43, 75.46 and 92.78% for the STCHOICE, CA-MARKOV and MLPNN simulations, respectively. Apart from the overall accuracies, the LULC class wise producer's and user's accuracies yielded better results in case of MLPNN modeling, while the same found worst in the case of STCHOICE modeling. Therefore, in the present study, the MLPNN approach performed best in all terms of model evaluation compared to the other two modeling approaches.
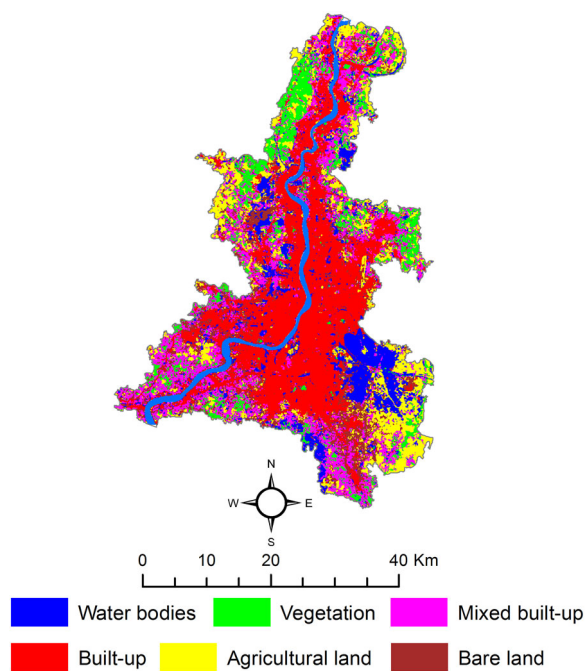
Figure 15. The MLPNN-Markov simulated LULC map of KMA for the year of 2016.
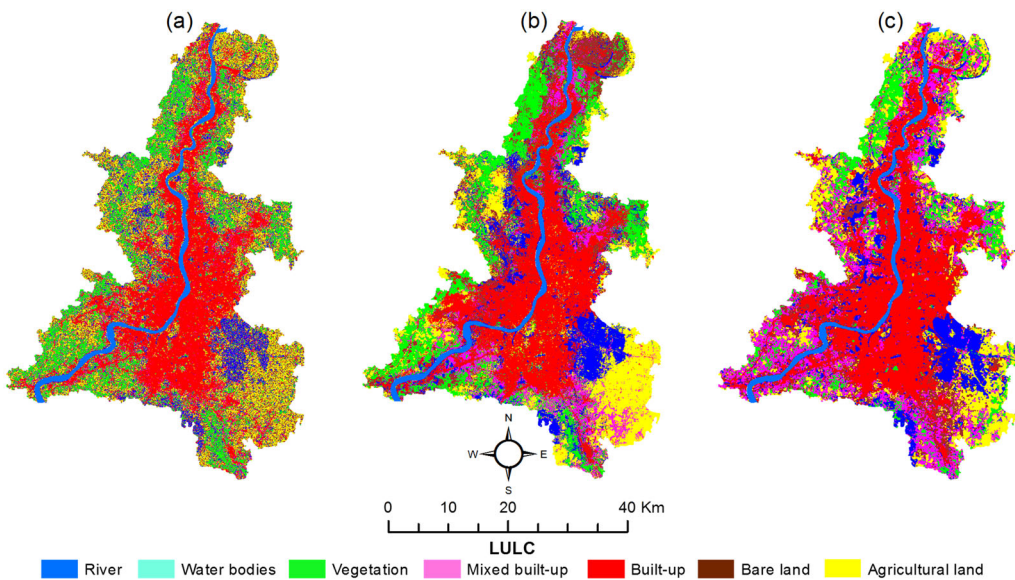
Figure 16. Three simulated LULC maps of KMA for 2016; (a) the STCHOICE model simulated LULC map of KMA for 2016; (b) the CA-MARKOV model simulated LULC map of KMA for 2016; and (c) the MLPNN model simulated LULC map of KMA for 2016.

4.5. Predicting future urban growth

The model validation reveals the MLPNN as the best-performed modeling approach in the present study. Hence, the MLPNN was employed for simulating future urban growth in KMA for the next two decades, that is, for 2036 (Figure 18). Finally, the spatial

Table 10. Per category wise comparison of the percentage of correct prediction (PCP) between actual and simulated maps of KMA (2016) for the three modeling approaches.

|	Actual (2016)		STCHOICE (2016)			CA-MARKOV (2016)			MLPNN (2016)		
	Area (Ha)	%	Area (Ha)	%	Error (%)	Area (Ha)	%	Error (%)	Area (Ha)	%	Error (%)
Water bodies	22919.94	13.29	20632.86	11.97	1.33	20621.16	11.96	1.33	20360.34	11.81	1.48
Vegetation	17354.16	10.07	28129.68	16.32	−6.25	30430.26	17.65	−7.58	17511.39	10.16	−0.09
Mixed built-up	30231.63	17.53	22483.53	13.04	4.49	16008.03	9.28	8.25	32211.27	18.68	−1.15
Built-up	54384.75	31.54	47821.41	27.74	3.81	52069.05	30.20	1.34	58011.84	33.65	−2.10
Agricultural land	25444.89	14.76	30456.09	17.67	−2.91	31670.01	18.37	−3.61	25793.46	14.96	−0.20
Bare land	22072.59	12.80	22884.39	13.27	−0.47	21609.45	12.53	0.27	18519.66	10.74	2.06
Total	172407.96	100	172407.96	100	0	172407.96	100	0	172407.96	100	0

Table 11. Summary of Kappa statistics and components of agreement and disagreement for the three modeling approaches: STCHOICE, CA-MARKOV and MLPNN.

Indices/components	STCHOICE model (2016)	CA-MARKOV model (2016)	MLPNN model (2016)
$K_{standard}$	0.5392	0.6941	0.9025
K_{no}	0.6494	0.7659	0.9258
$K_{location}$	0.6338	0.7678	0.9178
K_{histo}	0.8820	0.8270	0.9560
Fraction correct	0.4000	0.5490	0.8130
Agreement chance	0.1429	0.1429	0.1429
Agreement quantity	0.2050	0.2011	0.2049
Agreement grid cell	0.3517	0.4553	0.5886
Disagree grid cell	0.2032	0.1377	0.0527
Disagree quantity	0.0974	0.0630	0.0109
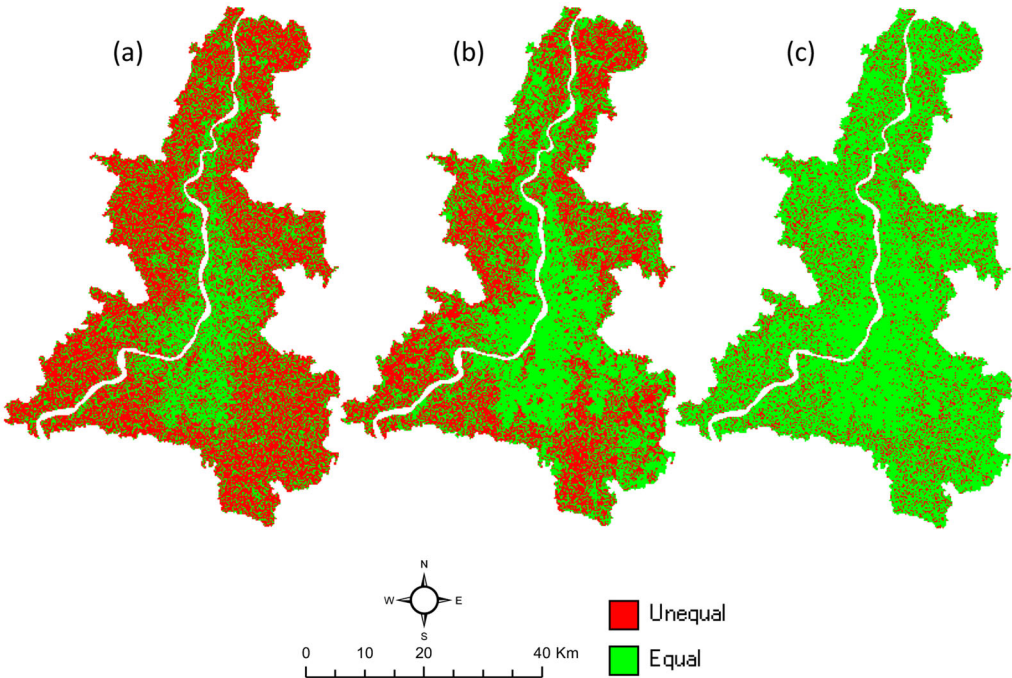
Figure 17. Cell-by-cell level of Kappa agreement between actual and simulated LULC maps of KMA (2016) for the three modeling techniques; (a) comparison for the STCHOICE modeling, (b) comparison for the CA-MARKOV modeling, and (c) comparison for the MLPNN modeling.
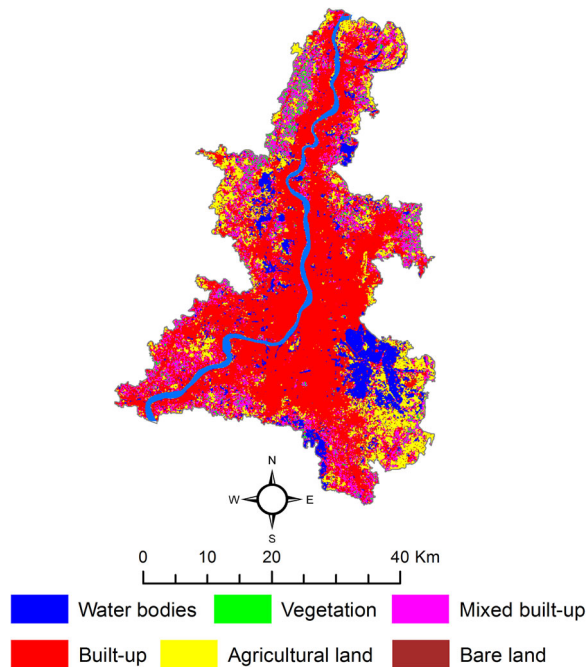
Figure 18. The MLPNN predicted future urban growth in KMA for 2036.

distribution of land covers, mainly built-up and mixed built-up covers in the simulated map, was examined applying a point pattern analysis (quadrat count tests and spatial Kolmogorov-Smirnov tests) for testing consistency of the simulation, as in Helbich (2012) and Shafizadeh-Moghadam and Helbich (2013). The result suggests a significant cluster pattern of the future built-up cover in KMA, which is better than random spatial distribution with $p < 0.001$.

The trends of land cover transition during 2006–2016 and 2016–2036 are presented in Table 12. As discussed earlier, diagonal elements of the matrices depict probability values for self-replacement, indicating land cover types to remain similar as present with respect to time; on the contrary, off-diagonal values represent probability values of change from one land cover to another category. During 2006–2016, the transition probability of changing into built-up remained higher, as found during 1996–2006 (Table 12). However, the probability of transition into mixed built-up from vegetation and bare land increased during 2006–2016 as compared to 1996–2006. Therefore, all the non-built-up covers depict a higher probability to change into built-up and mixed built-up covers during 2006–2016. Table 12 also presents the transition probability values of changing during the future 20 years, that is, from 2016 to 2036. The transition into built-up cover is likely to deepen during 2016–2036. The land covers like vegetation, barren land, water bodies reflect an increased probability to be converted into built-up areas. During the period, even mixed-built-up covers are also likely to be transformed into built-up covers (Table 13).

Figure 19 and Table 13 present class-wise changes in areas of the land covers during 1996–2006, 2006–2016 and 2016–2036. The results highlight that the share of built-up cover is predicted to increase from 31.54% in 2016 to 55.05% in 2036, amounting to an increase of about 24% at the cost of other non-built-up land covers, particularly bare land, agricultural land and vegetal cover. As a consequence, land covers like barren land,

Table 12. The MLPNN derived transition probability matrix presenting the probability of each land cover to change to other land covers during 2006–2016 and 2016–2036.

Period	LULCs	Water bodies	Vegetation	Mixed built-up	Built-up	Agricultural land	Bare land
2006–2016	Water bodies	0.455	0.0823	0.1168	0.0781	0.1167	0.1511
	Vegetation	0.0825	0.2931	0.3654	0.0426	0.0543	0.1621
	Mixed built-up	0.0001	0.0011	0.3817	0.6169	0.0002	0
	Built-up	0.0001	0.0004	0.1685	0.8302	0.0008	0
	Agricultural land	0.1558	0.0502	0.0902	0.0712	0.3899	0.2427
	Bare land	0.1069	0.0615	0.1917	0.1776	0.2467	0.2156
2016–2036	Water bodies	0.1472	0.1414	0.0994	0.3261	0.1681	0.1178
	Vegetation	0.1085	0.2571	0.135	0.2461	0.1432	0.11
	Mixed built-up	0.0002	0	0.0894	0.9104	0	0
	Built-up	0.0002	0	0.0241	0.9755	0.0001	0.0001
	Agricultural land	0.1463	0.1553	0.0734	0.1432	0.2979	0.1838
	Bare land	0.1335	0.1623	0.0811	0.1944	0.2626	0.1661

Table 13. Magnitude of areas (ha) under different land covers with a changing trend from 1996 to 2036 in the metropolitan of KMA.

	1996		2006		2016		2036	
LULC classes	Area (ha)	%	Area (ha)	%	Area (ha)	%	Area (ha)	%
Agricultural land	27423.18	15.85	27782.64	16.05	25444.89	14.76	23496.75	13.61
Bare land	22391.46	12.94	21190.86	12.24	22072.59	12.80	7464.69	4.32
Built-up	27781.65	16.05	41439.87	23.95	54384.75	31.54	95059.71	55.05
Mixed built-up	26995.68	15.60	27329.58	15.79	30231.63	17.53	25109.55	14.54
Vegetation	40090.86	23.17	32273.01	18.65	17354.16	10.07	4377.60	2.54
Water bodies	28381.05	16.40	23042.52	13.31	22919.94	13.29	17170.92	9.94
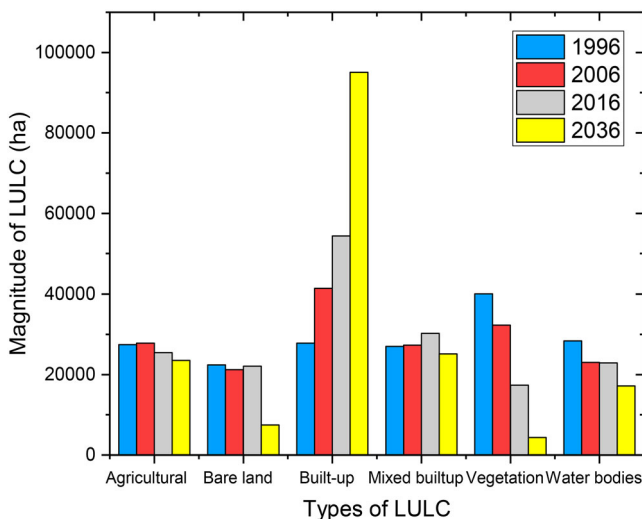
Figure 19. Present and future trend of change in the LULCs (ha) of KMA during 1996–2036.

vegetation, water bodies, and agricultural land are likely to sacrifice their areas up to 10% in the near future. The decadal built-up growth is expected to increase in the near future as compared to previous decades. The mixed built-up growth rate is predicted to decrease marginally as a result of large-scale conversion into built-up cover.

5. Discussion

Over the years, there has been a promising development in modeling urban growth and capturing the spatial and temporal dynamics of urban growth. A comparative modeling approach helps us to understand the strength and weaknesses of involved modeling techniques. The present study has adopted such a comparative approach, which deployed three RS-GIS integrated strategies, viz., STCHOICE, CA-MARKOV and MLPNN to model urban growth dynamics in KMA. First, each of the techniques was engaged to simulate the urban growth scenario for 2016. Based on the model validation results, the MLPNN integrated with MC was selected to predict future urban growth in KMA for 2036. The results of the PCP and Kappa agreement are found to be better for MLPNN modeling as compared to CA-MARKOV and STCHOICE techniques. The level of Kappa agreement between the actual and simulated land cover of 2016 is observed highest in the case of MLPNN modeling (0.9025) followed by CA-MARKOV (0.6941) and STCHOICE (0.5392) modeling, respectively.

The STCHOICE creates a stochastic land cover map by evaluating and conditional probabilities that each land cover exists at each pixel based on the past pattern of land cover change. In the Markovian process, a future prediction is a function of time where the future is predicted based on immediately preceding state, that is, present, without any consideration of spatiality or spatial contiguity. Urban growth is a complex spatial and temporal phenomenon where a large number of driving factors interplay. Thus, the relatively poor performance of the STCHOICE technique in the present study can be attributed to the lack of capturing spatial contiguity. On the other hand, the CA-MARKOV combines CA and MC analysis for modeling land cover change where the change of state of a pixel depends on time as well as state of the adjacent pixels in a defined space. It assumes that spatial configuration affects future land cover changes through interaction among locally defined land covers. The advantage of this kind of modeling is that the development of the suitability surface is based on MCE analysis. The MCE allows users to incorporate different socioeconomic and bio-physical factors and constraints for an objective under consideration. It also enables a user to standardize factors as per requirement and to weigh factors applying pairwise comparison procedure under the AHP framework. As a result, the CA-MARKOV modeling is widely applied in urban growth simulation for its simplicity, flexibility, intuitiveness, and ability to capture spatiotemporal processes (White and Engelen 1993; Sante et al. 2010; Eastman and Toledano 2018; Olmedo and Mas 2018). Therefore, in the present study, the CA-MARKOV could simulate the urban growth of KMA (2016) with a much higher precision as compared to STCHOICE in terms of the agreement between the simulated and actual scenarios.

Besides, the MLPNN is a popular ANN that inspires by the function of the brain and is a powerful non-linear model that predicts output data from a given input (Taud and Mas 2018). The MLPNN is a feed-forward neural network that has hidden layers between input and output layers and uses a BP algorithm based on information from training data. BP involves forward and backward propagations that are repeated iteratively until the error of the network minimizes to an acceptable level. The training of the network is accomplished with the objective to cultivate proper weights for both connections between input and hidden layers as well as hidden and output layers in order to classify unknown pixels (Atkinson and Tatnall 1997; Ahmed and Ahmed 2012). In the present research, a sum of nine transitions were modeled from non-built-up to mixed built-up and built-up applying the MLPNN modeling, in which a total of nineteen biophysical and socioeconomic explanatory variables were applied for each transition being modeled. In all cases, the obtained model training accuracies were around or more than 90%, with the skill

measure close to 0.9 or more and RMS about 0.1. Therefore, unlike the other two models, the MLPNN provides users a great deal of flexibility to train and validate each model or transition sub-model with a high level of accuracy. Besides, it also provides information about the contribution of each explanatory variable for each sub-model, including step-wise assessment through BP, which allows the user for an easy determination of most parsimonious model (Eastman and Toledano 2018).

The CA-MARKOV and MLPNN modeling reveal that proximity to built-up areas, proximity to metro stations, the likelihood of LULC class, proximity to town, and proximity to major roads are the primary drivers behind the urban expansion in KMA. Therefore, the local or proximity factors play major roles in the urban dynamics and expansion of the metropolitan.

KMA has witnessed incessant land consumption for urban built-up growth over time at the expense of non-urban covers. However, there is a significant difference in the rate of growth between urban (core) and peri-urban areas (Sahana et al. 2018; Rahaman et al. 2019). Positive growth in built-up cover and negative growth in mixed built-up cover characterize the KMA's statuary urban areas (core). However, along with the peri-urban areas, as a result of peripheral land consumption, the built-up and mixed-built-up areas are rapidly expanding. This enlightens the process of conversion of mixed built-up class into the built-up class around the periphery in KMA. It also demonstrates that the mixed built-up cover is mostly being converted to built-up cover in the central KMA, while along the peri-urban areas, all non-built-up class are largely being converted into mixed built-up class. The rate of land consumption along per-urban areas reflects an accelerated pace. The findings indicate that the KMA has been witnessing typical urban sprawl during recent years. On the one hand, unlike the central portion of KMA, which is getting more compact with time, the peri-urban areas are fast growing, featured by leapfrog and fragmented built-up development. In its report on SDG 11 and indicator 11.3.1, UN-Habitat (UN-Habitat, 2018a, 2018b), emphasized the benefits of compact urban development as opposed to sprawling. This study reveals that the urban as well as peri-urban areas do not have similar land consumption and land-use efficiency in respect to SDG indicator11.3.1. The central KMA reflects better land-use efficiency as a result of compact growth compared to the periphery reflecting leapfrog growth as a result of rapid urban sprawling.

The MLPNN-yielded future urban growth patterns for 2036 reveal that as a result of net loss in other LULCs including the mixed built-up cover, the built-up cover is anticipated to grow further. In the near future, the land covers such as vegetal cover, bare land, agricultural land, water bodies are likely to be affected mostly by this incessant concretization. Although built-up areas are proliferating in all directions around the metropolitan, particularly the regions towards the south and south-east are expected to be immensely concretized in the coming decades. Besides, around a net 3% loss in mixed built-up areas indicates further compact urban growth in KMA in the near future. Therefore, the central KMA is expected to be featured by a better LUE in the future compared to the present scenario as a result of further compact growth in the near future. However, the peri-urban areas are predicted to grow rapidly in the future as a result of further land consumption and conversion of non-built-up covers into mixed built-up cover. Therefore, there is a need for proper planning and policy framework, especially for the urban development over the peri-urban areas in KMA, to achieve overall sustainability as proposed in SDG indicator 11.3.1.

Since KMA is the largest metropolitan in eastern India, it attracts populations from all corners of West Bengal and neighboring states. Because of such ever-increasing urbanward migration in search of jobs, other opportunities, and a better standard of life, thousands of people are migrating to the metropolitan of KMA. The decadal population

growth analysis as studied by Cox (2012) confirms that a larger segment of the migrants prefer to settle along the peripheral part of KMA. Very high land value, higher apartment price, congestion, environmental pollution in the central part of the metropolitan on the one land and the provision of urban amenities in peripheral areas and recent development of some new township along the periphery of the metropolitan could be possible causes behind such pattern of urbanization. Moreover, residing at peripheral towns and townships, people can easily commute to the central part of the metropolitan for their daily livelihood and jobs, provided the high accessibility and connectivity prevailing in the metropolitan by means of the road, rail, metro and waterway and tram linkages. As a result, peripheral areas are booming with a mass concentration of population and therein concretization. The planning and developing solutions to challenges of complex urbanization as in KMA requires commitment and action on the part of a number of stakeholders identified by the UN who have a stake in the achievements of SDG 11.3. Integrated and sustainable planning and management for human settlement development along the peripheral regions are keys to achieve the SDG target 11.3 in KMA. This, in return, would result in better LCRPGR, particularly over the peri-urban areas required to achieve sustainable urbanization in KMA.

6. Conclusions

In this study, the spatiotemporal urban growth dynamics in KMA have been modeled in a comparative modeling framework employing three RS-GIS integrated techniques, namely STCHOICE, CA-MARKOV and MLPNN coupled with MC. The MLPNN modeling appears to be the most effective and efficient approach in simulating future urban scenarios compared to CA-MARKOV and STCHOICE, as the former over-performed the other two in the present study. The CA-MARKOV is also a widely used modeling approach in predicting future urban growth, particularly in the cases of Indian cities. However, the uniqueness of MLPNN, including the BP-driven linkages between input, hidden, and output nodes, makes it a reasonably better performer in simulate urban growth in a complex urban system. It also can simulate urban growth when the number of input variables is few or not sufficient. Hence, the MLPNN modeling could be effective for modeling urban growth in rapidly changing urban scenarios not just for KMA, but for all other cities in developing countries. However, the MLPNN modeling success is determined not only by the variables chosen, the number of hidden layers, nodes, and training data, but also by training parameters such as learning rate, number of iterations, and so on. Thus, the comparative modeling framework adopted in the present study may be useful in studies of urban growth modeling.

The inclusion of the selected biophysical and socio-economic variables has strengthened the results in the present modeling. The present study finds proximity to built-up or developed areas, distance metro, nearness to town or city, the empirical likelihood of land use, major road distance and railway distance are the most influential factors, while slope, elevation, distance from minor road, air quality index are least affecting factors. Therefore, the proximity and local factors play significant roles behind urban dynamics in KMA. However, the selection of explanatory variables has always been critical in such modeling studies. Hence, there always exists further scope to explore the better choice of a variable set to enhance the simulation performance.

The present study offers the first-ever implementation of modeling urban growth in whole KMA linking with urban land consumption and sustainability. Studies often investigate the present scenario of urban growth in a city to assess the LUE and LCRPGR.

Modeling urban growth offers to track the indicators both in the present and even with changing scenarios in the future. Moreover, the comparative modeling framework adopted in the present study can predict the changing scenario of land consumption with respect to SDG 11.3.1 with greater accuracy. Therefore, depending upon changing scenarios required for sustainable long-term urban planning, the current modeling approach may be helpful in allocating resources for the present and the future; hence, it may be useful for urban planning and policymaking. The present research finds that different LULCs in an urban system have a distinctive level of spatiotemporal dynamics and variability. Thus, the present modeling framework may also be helpful to the urban planner and policymakers to assess LUE and LCRPGR differently for different LULCs, for example, for built-up and mixed built-up covers separately. Accordingly, this modeling approach may help to formulate a policy framework in order to achieve sustainable urbanization better in cities as proposed in SDG target 11.3. Furthermore, the methodology can be easily adapted to other Indian cities.

7. Scope of future research

Limitations of present research work and future research directions are listed as follows.

- Only analysis and simulation of urban growth are not fruitful until the results are incorporated in urban planning and policy-making. Therefore, future research work may be conducted on policy formulation for future urban planning based on the outcome of the present research.
- The predicted pattern of future urban growth is dependent on the observed past and present land cover dynamics; hence, may change with changing scenarios in the future. Further research may be conducted in this regard.
- The present study used moderate resolution satellite images (30 m); therefore, the use of finer satellite images could result in better accuracy.
- The present study considered a 20-year study period. More extended time-series data may be used for understanding further dynamics (if any).

Note

1. A Census town is one which is not statutorily notified and administered as a town, but nevertheless attained urban characteristics as defined by the Census of India.

Disclosure Statement

No potential conflict of interest was reported by the author(s).

ORCID

Sk Mithun 🅳 http://orcid.org/0000-0002-1749-1382
Romulus Costache 🅳 http://orcid.org/0000-0002-6876-8572

References

Abiden MZZ, Abidin SZ, Jamaluddin MNF. 2010. Pixel based urban growth model for predicting future pattern. In 2010 6th International Colloquium on Signal Processing & Its Applications. IEEE; p. 1–5.

Aburas MM, Ho YM, Ramli MF, Ash'aari ZH. 2017. Improving the capability of an integrated CA-Markov model to simulate spatio-temporal urban growth trends using an Analytical Hierarchy Process and Frequency Ratio. Int J Appl Earth Obs Geoinf. 59:65–78.

Ahmed B. 2011. Urban land cover change detection analysis and modelling spatio-temporal growth dynamics using remote sensing and GIS techniques: A case study of Dhaka, Bangladesh. Retrieved from https://run.unl.pt/bitstream/10362/8298/1/TGEO0061.pdf.

Ahmed B, Ahmed R. 2012. Modeling urban land cover growth dynamics using multi-temporal satellite images: A case study of Dhaka, Bangladesh. IJGI. 1(1):3–31.

Al-Ahmadi K, See L, Heppenstall A, Hogg J. 2009. Calibration of a fuzzy cellular automata model of urban dynamics in Saudi Arabia. Ecol Complex. 6(2):80–101.

Almeida CD, Gleriani JM, Castejon EF, Soares-Filho BS. 2008. Using neural networks and cellular automata for modelling intra-urban land-use dynamics. Int J Geogr Inf Sci. 22(9):943–963.

Al-Sharif AA, Pradhan B. 2014. Urban sprawl analysis of Tripoli Metropolitan city (Libya) using remote sensing data and multivariate logistic regression model. J Indian Soc Remote Sens. 42(1):149–163.

Anderson JR. 1976. A land use and land cover classification system for use with remote sensor data (Vol. 964). Washington, DC: US Government Printing Office.

Araya YH, Cabral P. 2010. Analysis and modeling of urban land cover change in Setúbal and Sesimbra, Portugal. Remote Sens. 2(6):1549–1563.

Arsanjani JJ, Helbich M, de Noronha Vaz E. 2013. Spatiotemporal simulation of urban growth patterns using agent-based modeling: The case of Tehran. Cities. 32:33–42.

Atkinson PM, Tatnall AR. 1997. Introduction neural networks in remote sensing. Int J Remote Sens. 18(4):699–709.

Barredo JI, Kasanko M, McCormick N, Lavalle C. 2003. Modelling dynamic spatial processes: simulation of urban future scenarios through cellular automata. Landsc Urban Plann. 64(3):145–160.

Batty M. 2009. Cities as complex systems: scaling, interaction, networks, dynamics and urban morphologies. In Meyers R., editor. Encyclopedia of complexity and systems science. New York, NY: Springer.

Batty M. 2005. Agents, cells, and cities: new representational models for simulating multiscale urban dynamics. Environ Plan A. 37(8):1373–1394.

Batty M, Longley PA. 1994. Fractal cities: a geometry of form and function. London (UK): Academic Press.

Batty M, Xie Y. 1994. From cells to cities. Environ Plann B Plann Des. 21(7):S31–S48.

Batty M, Xie Y, Sun Z. 1999. Modeling urban dynamics through GIS-based cellular automata. Comput Environ Urban Syst. 23(3):205–233.

Behera MD, Borate SN, Panda SN, Behera PR, Roy PS. 2012. Modelling and analyzing the watershed dynamics using Cellular Automata (CA)-Markov model - A geo-information based approach. J Earth Syst Sci. 121(4):1011–1024.

Berling-Wolff S, Wu J. 2004. Modeling urban landscape dynamics: a case study in Phoenix, USA. Urban Ecosyst. 7(3):215–240.

Bhatta B. 2012. Urban growth analysis and remote sensing: a case study of Kolkata, India 1980–2010. Dordrecht (Netherlands): Springer Science & Business Media.

Bhatta B. 2013. Research methods in remote sensing. Dordrecht (Netherlands): Springer.

Clarke KC, Hoppen S, Gaydos L. 1997. A self-modifying cellular automaton model of historical urbanization in the San Francisco bay area. Environ Plann B. 24(2):247–261.

Cox W. 2012. *The Evolving Urban Form: Kolkata: 50 Mile City* | Newgeography.com, 1–7. Retrieved from http://www.newgeography.com/content/002620-the-evolving-urban-form-kolkata-50-mile-city.

Devendran AA, Lakshmanan G. 2019. Analysis and prediction of urban growth using neural-network-coupled agent-based cellular automata model for Chennai metropolitan area, Tamil Nadu, India. J Indian Soc Remote Sens. 47(9):1515–1526.

Dhali MK, Chakraborty M, Sahana M. 2019. Assessing spatio-temporal growth of urban sub-centre using Shannon's entropy model and principle component analysis: a case from North 24 Parganas, lower Ganga River Basin, India. Egypt J Remote Sens Space Sci. 22(1):25–35.

Eastman JR. 1999. Guide to GIS and image processing (Volume 1). Worcester, MA: Clark Labs, Clark University.

Eastman JR. 2015. TerrSet: Geospatial monitoring and modeling system. Worcester, MA, USA: Clark University.

Eastman JR, Toledano J. 2018. A short presentation of the Land Change Modeler (LCM). In Geomatic approaches for modeling land change scenarios. Cham: Springer; p. 499–505.

Eastman JR, Jiang H, Toledano J, et al. 1998. Multi-criteria and multi-objective decision making for land allocation using GIS. In Beinat E., editor, Multicriteria analysis for land-use management. Dordrecht: Springer; p. 227–251.

Eastman JR, Van Fossen ME, Solarzano LA. 2005. Transition potential modeling for land cover change. In: Maguire, D.J., Goodchild, M.F. and Batty, M., editors, GIS, spatial analysis and modeling, ESRI Press, p. 357–386.

Eastman JR, Jin W, Kyem PAK, Toledano J. 1995. Raster procedures for multi-criteria/multi-objective decisions. Photogramm Eng Remote Sens. 61(5):539–547.

Estoque RC, Murayama Y. 2014. Measuring sustainability based upon various perspectives: a case study of a hill station in Southeast Asia. Ambio. 43(7):943–956.

Estoque RC, Ooba M, Togawa T, Hijioka Y, Murayama Y. 2021. Monitoring global land-use efficiency in the context of the UN 2030 Agenda for Sustainable Development. Habitat Int. 115:102403.

Fang S, Gertner GZ, Sun Z, Anderson AA. 2005. The impact of interactions in spatial simulation of the dynamics of urban sprawl. Landsc Urban Plann. 73(4):294–306.

Ganesan VB. 2016. The planning behind the City of Joy. The Hindu. https://www.thehindu.com/books/the-planning-behind-the-city-of-joy/article3394580.ece.

Helbich M. 2012. Beyond postsuburbia? Multifunctional service agglomeration in Vienna's urban fringe. Tijdschr Econ Soc Geogr. 103(1):39–52.

Herold M, Goldstein NC, Clarke KC. 2003. The spatiotemporal form of urban growth: measurement, analysis and modeling. Remote Sens Environ. 86(3):286–302.

Hu X, Weng Q. 2009. Estimating impervious surfaces from medium spatial resolution imagery using the self-organizing map and multi-layer perceptron neural networks. Remote Sens Environ. 113(10):2089–2102.

Hu Z, Lo CP. 2007. Modeling urban growth in Atlanta using logistic regression. Comput Environ Urban Syst. 31(6):667–688.

Jalilov SM, Chen Y, Quang NH, Nguyen MN, Leighton B, Paget M, Lazarow N. 2021. Estimation of urban land-use efficiency for sustainable development by integrating over 30-year Landsat imagery with population data: a case study of ha long, Vietnam. Sustainability. 13(16):8848.

Jat MK, Choudhary M, Saxena A. 2017. Urban growth assessment and prediction using RS, GIS and SLEUTH model for a heterogeneous urban fringe. Egypt J Remote Sens Space Sci. 10(3):1–19.

Jjumba A, Dragićević S. 2012. High resolution urban land-use change modeling: Agent iCity approach. Appl Spatial Anal. 5(4):291–315.

KMDA 2011. KMDA annual report. http://www.kmdaonline.org/html/aar_2011.php.

Laituri M, Davis D, Sternlieb F, Galvin K. 2021. SDG Indicator 11.3. 1 and secondary cities: an analysis and assessment. IJGI. 10(11):713.

Lambin EF. 2004. Modelling land-use change. In Wainwright, J. & Mulligan, M. (Eds) Environmental modeling: finding simplicity in complexity. Chichester, UK: John Wiley & Sons; p. 245–254

Landis JD. 1995. Imagining land use futures: applying the California urban futures model. J Am Plann Assoc. 61(4):438–457.

Li C, Cai G, Du M. 2021. Big data supported the identification of urban land Efficiency in Eurasia by indicator SDG 11.3. 1. IJGI. 10(2):64.

Li X, Yeh AGO. 2000. Modelling sustainable urban development by the integration of constrained cellular automata and GIS. Int J Geogr Inf Sci. 14(2):131–152.

Liu Y. 2008. Modelling urban development with geographical information systems and cellular automata. New York: CRC Press.

Liu Y. 2012. Modelling sustainable urban growth in a rapidly urbanising region using a fuzzy-constrained cellular automata approach. Int J Geogr Inf Sci. 26(1):151–167.

Maithani S. 2009. A neural network based urban growth model of an Indian city. J Indian Soc Remote Sens. 37(3):363–376.

Malczewski J, Chapman T, Flegel C, Walters D, Shrubsole D, Healy MA. 2003. GIS–multi-criteria evaluation with ordered weighted averaging (OWA): case study of developing watershed management strategies. Environ Plan A. 35(10):1769–1784.

Melchiorri M, Pesaresi M, Florczyk AJ, Corbane C, Kemper T. 2019. Principles and applications of the global human settlement layer as baseline for the land use efficiency indicator—SDG 11.3. 1. IJGI. 8(2):96.

Mishra VN, Rai PK. 2016. A remote sensing aided multi-layer perceptron-Markov chain analysis for land use and land cover change prediction in Patna district (Bihar), India. Arab J Geosci. 9:249.

Mithun S. 2020. Quantifying and modeling metropolitan growth dynamics: A case study on Kolkata Metropolitan Area [Doctoral dissertation]. IIT Kharagpur.

Mithun S, Chattopadhyay S, Bhatta B. 2016. Analyzing urban dynamics of metropolitan Kolkata, India by using landscape metrics. Papers Appl Geogr. 2(3):284–297.

Mithun S, Sahana M, Chattopadhyay S, Johnson BA, Khedher KM, Avtar R. 2021. Monitoring metropolitan growth dynamics for achieving sustainable urbanization (SDG 11.3) in Kolkata Metropolitan Area, India. Remote Sens. 13(21):4423.

Mondal B, Chakraborti S, Das DN, Joshi PK, Maity S, Pramanik MK, Chatterjee S. 2020. Comparison of spatial modelling approaches to simulate urban growth: a case study on Udaipur city, India. Geocarto Int. 35(4):411–433.

Mondal B, Das DN, Bhatta B. 2017. Integrating cellular automata and Markov techniques to generate urban development potential surface: A study on Kolkata agglomeration. Geocarto Int. 32(4):401–419.

Mondal B, Das DN, Dolui G. 2015. Modeling spatial variation of explanatory factors of urban expansion of Kolkata: A geographically weighted regression approach. Model Earth Syst Environ. 1(4):29.

Munshi T, Zuidgeest M, Brussel M, van Maarseveen M. 2014. Logistic regression and cellular automata-based modelling of retail, commercial and residential development in the city of Ahmedabad, India. Cities. 39:68–86.

Nong Y, Du Q. 2011. Urban growth pattern modeling using logistic regression. Geo-Spatial Inf Sci. 14(1):62–67.

Olmedo MC, Mas JF. 2018. Cellular automata in CA_MARKOV. In Geomatic approaches for modeling land change scenarios. Cham: Springer; p. 425–428

Park S, Jeon S, Choi C. 2012. Mapping urban growth probability in South Korea: Comparison of frequency ratio, analytic hierarchy process, and logistic regression models and use of the environmental conservation value assessment. Landsc Ecol Eng. 8(1):17–31.

Park S, Jeon S, Kim S, Choi C. 2011. Prediction and comparison of urban growth by land suitability index mapping using GIS and RS in South Korea. Landsc Urban Plann. 99(2):104–114.

Pontius RG. 2000. Quantification error versus location error in comparison of categorical maps. Photogramm Eng Remote Sens. 66(8):1011–1016.

Pooyandeh M, Mesgari S, Alimohammadi A, Shad R. 2007. A comparison between complexity and temporal GIS models for spatio-temporal urban applications. In International Conference on Computational Science and Its Applications. Berlin: Springer; p. 308–321

Rahaman M, Dutta S, Sahana M, Das DN. 2019. Analysing urban sprawl and spatial expansion of Kolkata urban agglomeration using geospatial approach. In Applications and challenges of geospatial technology. Cham: Springer; p. 205–221.

Rienow A, Kantakumar LN, Ghazaryan G, Dröge-Rothaar A, Sticksel S, Trampnau B, Thonfeld F. 2022. Modelling the spatial impact of regional planning and climate change prevention strategies on land consumption in the Rhine-Ruhr Metropolitan Area 2017–2030. Landsc Urban Plann. 217:104284.

RC, PK, Maithani S. 2014. Modelling urban growth in the Indo-Gangetic plain using nighttime OLS data and cellular automata. Int J Appl Earth Obs Geoinf. 33(1):155–165.

Saaty TL. 1977. A scaling method for priorities in hierarchical structures. J Math Psychol. 15(3):234–281.

Sahana M. 2018. Analyzing urban spatial patterns and trend of urban growth using urban sprawl matrix: A study on Kolkata urban agglomeration, India. Sci. Total Environ. 628:1557–1566.

Sahana M, Dutta S, Sajjad H. 2019. Assessing land transformation and its relation with land surface temperature in Mumbai city, India using geospatial techniques. Int J Urban Sci. 23(2):205–225.

Sahana M, Hong H, Sajjad H. 2018. Analyzing urban spatial patterns and trend of urban growth using urban sprawl matrix: A study on Kolkata urban agglomeration, India. Sci Total Environ. 628:1557–1566.

Sante I, García AM, Miranda D, Crecente R. 2010. Cellular automata models for the simulation of real-world urban processes: A review and analysis. Landscape Urban Plann. 96(2):108–122.

Schiavina M, Melchiorri M, Corbane C, Florczyk AJ, Freire S, Pesaresi M, Kemper T. 2019. Multi-scale estimation of land use efficiency (SDG 11.3. 1) across 25 years using global open and free data. Sustainability. 11(20):5674.

Shafizadeh-Moghadam H, Helbich M. 2013. Spatiotemporal urbanization processes in the megacity of Mumbai, India: A Markov chains-cellular automata urban growth model. Appl Geogr. 40:140–149.

Shafizadeh-Moghadam H, Minaei M, Pontius RG, Jr, Asghari A, Dadashpoor H. 2021. Integrating a forward feature selection algorithm, random forest, and cellular automata to extrapolate urban growth in the Tehran-Karaj Region of Iran. Comput Environ Urban Syst. 87:101595.

Sharda R. 1994. Neural networks for the MS/OR analyst: an application bibliography. Interfaces. 24(2):116–130.

Sudhira HS, Ramachandra TV, Jagadish KS. 2004. Urban sprawl: metrics, dynamics and modelling using GIS. Int J Appl Earth Obs Geoinf. 5(1):29–39.

Takada T, Miyamoto A, Hasegawa SF. 2010. Derivation of a yearly transition probability matrix for land-use dynamics and its applications. Landsc Ecol. 25(4):561–572.

Tang J, Wang L, Yao Z. 2007. Spatio-temporal urban landscape change analysis using the Markov chain model and a modified genetic algorithm. Int J Remote Sens. 28(15):3255–3271.

Taud H, Mas JF. 2018. Multi-layer perceptron (MLP). In Geomatic approaches for modeling land change scenarios. Cham: Springer; p. 451–455.

UN-Habitat 2016. Indicator 11.3.1: Ratio of land consumption rate to population growth rate. Version 19 July 2016. Nairobi: United Nations Human Settlements Programme (UN-Habitat).

UN-Habitat 2018a. SDG indicator 11.3.1 training module: Land use efficiency. Nairobi: United Nations Human Settlement Programme (UN-Habitat).

UN-Habitat 2018b. SDG 11 synthesis report 2018: Tracking progress towards inclusive, safe, resilient and sustainable cities and human settlements. Nairobi: United Nations Human Settlement Programme (UN-Habitat).

Wang Y, Huang C, Feng Y, Zhao M, Gu J. 2020. Using earth observation for monitoring SDG 11.3. 1-ratio of land consumption rate to population growth rate in Mainland China. Remote Sens. 12(3): 357.

White R, Engelen G. 1993. Cellular automata and fractal urban form: A cellular modelling approach to the evolution of urban land-use patterns. Environ Plan A. 25(8):1175–1199.

Wu F, Webster CJ. 1998. Simulation of land development through the integration of cellular automata and multi-criteria evaluation. Environ Plann B. 25(1):103–126.

Xie Y. 2010. A generalized model for cellular urban dynamics. Geogr Anal. 28(4):350–373.

Zhang Q. 2009. Spatial-temporal patterns of urban growth in Shanghai, China: Monitoring, analysis, and simulation [Doctoral dissertation]. KTH Royal Institute of Technology.